J. Fluid Mech. (1992), *vol.* 238, *pp.* 599–632
Printed in Great Britain

Quasi-periodic and chaotic flow regimes in a thermally driven, rotating fluid annulus

By P. L. READ†, M. J. BELL, D. W. JOHNSON AND R. M. SMALL

Meteorological Office, London Road, Bracknell, Berkshire, UK

(Received 31 January 1991 and in revised form 6 November 1991)

Results are presented from analyses of high-precision time series of measurements of temperature and total heat transport obtained in a high-Prandtl-number ($Pr = 26$) fluid contained in a rotating, cylindrical annulus subject to a horizontal temperature gradient. Emphasis is placed on regions of parameter space close to the onset of irregular and/or chaotic behaviour. Two distinct transitions from oscillatory to apparently chaotic flow have been identified. The first occurs in an isolated region of parameter space at moderate to high Taylor number in association with a transition to a lower azimuthal wavenumber, in which a quasi-periodic ($m = 3$) amplitude vacillation (on a 2-torus) gives way to a low-dimensional ($D \sim 3$) chaotically modulated vacillation at very low frequency (apparently organized about a 3-torus). The spatial structure of the chaotic flow exhibits the irregular growth and decay of azimuthal sidebands suggestive of a nonlinear competition between adjacent azimuthal wavenumbers. The other main transition to aperiodic flow occurs at high Taylor number as the stability parameter Θ is decreased, and is associated with the onset of 'structural vacillation'. This transition appears to be associated with the development of small-scale instabilities within the main $m = 3$ baroclinic wave pattern, and exhibits a route to chaos via intermittency. The nature of the apparent chaos in these two aperiodic regimes is discussed in relation to possible mechanisms for deterministic chaos, apparatus limitations, and to previous attempts to model nonlinear baroclinic waves using low-order spectral models.

1. Introduction

Baroclinic waves are typical features of the stably stratified mid-latitude circulation of the atmosphere, where they contribute strongly to the poleward and vertical transport of heat and momentum, and release potential energy associated with the large-scale horizontal (equatorward) temperature gradient. Essentially the same wave-like features are also of importance in the oceans, and the atmospheres of planets other than the Earth. These disturbances are some of the most energetic components of the atmospheric circulation, and it is widely recognized that the predictability of the atmosphere is strongly dependent upon the detailed behaviour of the fully developed forms of these waves.

Attempts to model and study the dynamics of fully developed baroclinic waves are fraught with mathematical difficulties because of the strong intrinsic nonlinearities due to the advection of momentum, vorticity and temperature. In this context,

† Present address: Robert Hooke Institute, Clarendon Laboratory, Parks Road, Oxford, OX1 3PU, UK

laboratory studies of free thermal convection in a cylindrical fluid annulus, differentially heated in the horizontal and rotated about its (vertical) axis of symmetry, have been a valuable source of insight (e.g. Hide & Mason 1975). The flow in such a system is well known to exhibit a wide variety of distinct regimes, depending upon the imposed external conditions. Such regimes include steady axisymmetric flows, and non-axisymmetric flows which may be either spatially regular and steady or quasi-periodic in time, or spatially irregular and aperiodic in time. The axisymmetric flows largely consist of laminar overturning motions concentrated into boundary layers, while non-axisymmetric flows are dominated in the quasi-geostrophic interior by fully developed baroclinic waves (Hide & Mason 1975).

In attempting to account for the rich variety of flow regimes exhibited in the rotating annulus (e.g. see Hignett *et al.* 1985; hereafter referred to as HWCJS), much theoretical work has been concentrated on linear and weakly nonlinear mathematical models, frequently (though not necessarily) based on quasi-geostrophic theory (e.g. Pedlosky 1987). Linear theory can give useful insight into the conditions under which the axisymmetric regime will occur, and has shown that baroclinic waves will grow via an instability of the axisymmetric flow with wave structures which are often similar to observed disturbances. Weakly nonlinear theory focuses attention upon supercritical conditions close to the onset of instability, where only one or two wave components may be linearly unstable. Various analyses have considered the equilibration of unstable baroclinic waves, either to steady or periodically vacillating states (e.g. see Hart 1979 for a review). Further analyses (e.g. Gibbon & McGuinness 1980; Pedlosky & Frenzen 1980; Brindley & Moroz 1980) have even indicated ways in which flows with very simple spatial structure (e.g. a single wave and a zonal flow) may undergo transitions to aperiodic, chaotic behaviour. Under certain conditions, the amplitude equations reduce to the classical three-component Lorenz (1963*a*) equations.

Under more strongly supercritical conditions, theoretical studies have tended to follow Lorenz (1963*b*) in studying the behaviour of fully nonlinear, though severely spectrally truncated, quasi-geostrophic numerical models. It has long been recognized that such models are capable of exhibiting flow regimes with several aspects apparently in common with laboratory systems, such as regular waves, periodic vacillations and irregular flow. The extent to which such models account for the experimentally observed flow regimes in detail, however, remains unclear. A further problem with severely truncated spectral models is that the occurrence of certain regimes, notably involving low-dimensional chaos, may be strongly dependent upon the level of truncation (e.g. Nese, Dutton & Wells 1987; Curry *et al.* 1984). Such a problem is of even greater concern regarding the frequent application of truncated spectral models in the interpretation of atmospheric phenomena (e.g. Cehelsky & Tung 1987).

Laboratory studies may have an important role as a physical means of testing and verifying such interpretive models and their convergence properties. Hart and co-workers have made considerable progress in studying the transition to 'baroclinic chaos' in rotating two-layer experiments, and in trying to relate their results to the behaviour of various types of low-order model (e.g. Hart 1985, 1986; Ohlsen & Hart 1989*a*, *b*), with experimental evidence for routes involving period-doubling cascades and quasi-periodicity. Despite a longer tradition of experimental studies, similar work on the transition to disordered flow in the thermal annulus does not seem to have progressed quite so rapidly. Guckenheimer & Buzyna (1983) investigated the

apparent increase in attractor dimension as the rotation rate was increased, taking the system into the so-called 'geostrophic turbulence' regime, but did not investigate the properties of their reconstructed attractors in much detail. Most other reported studies have been concerned primarily with the spectral properties of the flow (both spatial and temporal) in the well-known irregular regime (e.g. Buzyna, Pfeffer & Kung 1984), with rather less attention directed towards characterizing the onset of 'weak turbulence' and chaos.

In the present work, we concentrate upon regions in parameter space close to the initial onset of aperiodic behaviour, but in which the spatial structure remains relatively simple. Although some of the flows considered may be related to the well-known irregular regime, in the present paper we do not discuss the properties of fully developed irregular flow. Various methods are used to characterize the flows obtained, including spectral methods and attractor reconstruction techniques. The latter are particularly demanding of data quality and quantity, and of standards of experimental control. Accordingly, even though we are dealing with a well-studied experimental configuration, the use of these analysis techniques has required the development of an experimental and data acquisition strategy which is a considerable improvement on previous studies. Section 2 describes the technical details of the apparatus and analysis methods. Section 3 presents an overview of the main flow regimes encountered in the experiments, including a novel aperiodic doubly modulated travelling wave flow, and the properties of the reconstructed attractors, elucidating each main flow type by comparison. The nature and particular characteristics of each regime are discussed in more detail in §4, and the significance of the new results is discussed in §5.

2. Apparatus and data reduction

The apparatus consisted of a rotating annulus of conventional design, and was essentially the same as described by Hignett (1982, 1985; hereafter referred to as H82 and H85 respectively) and HWCJS. The working fluid was contained in the annular gap between two upright coaxial brass cylinders of radii $r = 2.5$ cm and 8.0 cm, and two rigid, insulating horizontal boundaries in contact with the fluid at $z = 0$ and 14.0 cm. The apparatus was rotated about its vertical axis of symmetry and differentially heated horizontally at the sidewalls (the outer cylinder being the warmer). The annulus was levelled to within 10^{-4} rad and mounted on a turntable driven directly by a servo-controlled permanent magnet d.c. motor with a stability of about 1 part in 10^4. The working fluid consisted of a 25% solution by volume of glycerol in water, with a mean density of 1.081 g cm^{-3} at 20 °C, kinematic viscosity ν of 3.18×10^{-2} cm^2 s^{-1}, thermal diffusivity κ of 1.20×10^{-3} cm^2 s^{-1} and Prandtl number $Pr\,(=\nu/\kappa)$ of 26.4. Inhomogeneities in temperature across each side boundary were less than 2% of the applied temperature difference, and wall temperatures were kept constant in time typically to ± 0.02 K.

The annulus was designed for the precision measurement of fluid and boundary temperatures (via thermocouples), and of total heat transport. Temperatures at the boundaries and in the fluid were measured using copper–constantan thermocouples (sensitivity ~ 40 μV per K). In the fluid, 32 thermocouples were equally spaced azimuthally at mid-height and mid-radius, enabling the wavenumber spectrum to be obtained readily by fast Fourier transform techniques. The total heat transport through the inner side boundary was measured using the method described by H82 and HWCJS from the coolant (water) flow rate and the difference in temperature

between the inset and outlet. Use of a spiral channel adjacent to the inner cylinder to circulate the coolant kept the thermal time constant for the measurement of heat transport to no more than ~ 8–10 s. The convection chamber and associated components were operated in a thermostatically controlled enclosure and, by using the procedures detailed by H82, total heat transport could be measured to an absolute precision of $\sim \pm 2\%$, though much smaller relative changes ($\sim$ parts in 10^3) could be detected.

A variety of different procedures were used to take in and analyse the data. Short time series of measurements at all thermocouples in the fluid and boundaries, and of the total heat transport, scanned nearly simultaneously at 25 readings per second by a reed relay scanner, were recorded and used to identify the dominant flow type and to measure the wave drift rates and (where appropriate) vacillation frequencies (e.g. see H85). This method was used over a wide region of the regime diagram to map the occurrence of principal flow types, using both impulsive spin-up starts and slow changes in rotation rate at constant temperature difference to explore all possible flow types occurring in a given region of parameter space. At selected points, much longer, high-precision time series of temperature at one of the ring thermocouples and the total heat transport were recorded for up to 250 drift periods (requiring up to 20 h of measurements) for subsequent analysis. To minimize the effects of scanner noise and other unwanted effects, the temperature at a single thermocouple and heat flow were scanned continuously at 25 readings per s and averages over 1–2 s were recorded. For each flow for which a long single-point time series was measured, a contiguous short sequence of data at all thermocouples was also taken as above to assist with the characterization of the spatial properties of the flow.

The long time series were required both for high-resolution power spectral analysis and for the reconstruction of 'phase portraits' by the 'method of delays' (e.g. Takens 1980; Eckman & Ruelle 1985). In the latter, a scalar time series $T(t)$ is represented as a trajectory in a K-dimensional embedding space by denoting the state of the flow at time t by the vector $[T(t), T(t+\tau), T(t+2\tau) \ldots T(t+(K-1)\tau)]$. Given enough data at a representative point in the flow and an appropriate choice of the delay time τ, the time series generates a trajectory which lies on a manifold which is topologically equivalent to one in true phase space on which the attractor for the flow lies (Takens 1980). From such a reconstructed 'attractor', various invariant properties, such as estimates of attractor dimension and Lyapunov exponents, can (at least in principle) be derived (e.g. Eckmann & Ruelle 1985). Some examples of the calculation of such estimates from temperature and heat flow measurements are discussed below in §3.

In the present work, phase portrait reconstruction was further refined by the use of singular value decomposition (SVD – Broomhead & King 1986) to reproject the trajectory onto a statistically optimal orthogonal basis. As discussed by Broomhead & King (1986), this method eliminates some of the arbitrary choices to be made in time-delay embedding (e.g. of delay time τ). Use of a truncated set of the derived eigenvectors also introduces a useful element of filtering which can remove some of the unwanted non-deterministic components of the signal. For the present work, time series were typically sampled at 1.5–2 s intervals, placing 200 or more samples per wave drift period (though rather fewer per typical vacillation period, which ranged typically from 50–300 s). Most of the phase portraits displayed and analysed below were obtained using SVD with a 'window' of 50 points sampled every timestep of the original time series; i.e. a [50, 1] window in the terminology of Broomhead & King (1986). Estimates of invariants such as dimension and the dominant Lyapunov exponent were typically derived from the SVD-projected trajectories.

3. Identification of chaotic regimes

3.1. *Regime diagram* (*figure* 1)

Before embarking upon a detailed study of particular flows and transitions, it is important to establish an appropriate regime diagram showing the regions of parameter space in which particular flow types are observed to occur. With the thermal annulus, flow regimes are commonly ordered with respect to two principal dimensionless parameters, found empirically to be the most important in determining the observed flow type; namely (*a*) a stability parameter (sometimes referred to as a Burger or thermal Rossby number) Θ, defined by

$$\Theta = \frac{g\alpha\Delta T D}{[\Omega(b-a)]^2}, \tag{3.1}$$

(where g is the acceleration due to gravity, α the volumetric expansion coefficient, ΔT the imposed thermal contrast, Ω the system rotation rate, and D, a and b the annulus depth, inner and outer radius respectively); and (*b*) a Taylor number, usually defined by

$$\mathscr{T} = \frac{4\Omega^2(b-a)^5}{\nu^2 D} \tag{3.2}$$

(where ν is the kinematic viscosity). The regime diagram obtained in the present study is shown in figure 1. The dominant azimuthal wavenumber, m, of each flow is indicated by a number and the flow type by qualifying letters. Sharp transitions between regimes of different azimuthal wavenumber are marked as solid curves, and between regimes of the same m by thick dashed curves. Less sharply defined transitions are indicated by dotted lines.

In common with other studies of baroclinic waves in the rotating annulus (e.g. Hide & Mason 1975), the incidence of multiple equilibria is widespread, in the sense that more than one wavenumber and/or flow type is obtainable at a given point in parameter space. Every type of flow obtained within the region of parameter space investigated is shown in figure 1. The flow obtained depends largely upon the initial conditions and the way the experimental conditions were approached. Regular wave flows are either found to be steady (apart from a slow azimuthal drift of a constant flow pattern around the apparatus) or to vary periodically in amplitude and/or structure in a form of behaviour which is frequently referred to as 'vacillation'. Two main types of vacillation are widely reported in studies of rotating annulus convection (e.g. Hide & Mason 1975), namely 'amplitude vacillation' (AV) and 'structural vacillation' (SV). In the former, the principal manifestation is that of a regular symmetric wave pattern oscillating periodically in amplitude, but with little change of form. Various authors have also noted more subtle effects such as asymmetries between the growth and decay rate of the dominant wave, and modulations of the drift rate of the wave synchronous with the modulation of wave amplitude, and the precise nature of this phenomenon is still a matter of some controversy (e.g. contrast H85 and Buzyna, Pfeffer & Kung 1989). In structural vacillation the dominant wavenumber component remains at nearly constant amplitude but oscillates in structure or orientation. These oscillations may be periodic or irregular and a variety of characteristics have been reported (cf. Hide & Mason 1975; Pfeffer, Buzyna & Kung 1980; HWCJS). The onset of SV appears to signal the early stages of the development of fully irregular flow, in which the dominant wavenumber and flow structure varies erratically in a form of 'geostrophic turbulence' (e.g. Buzyna *et al.* 1984).

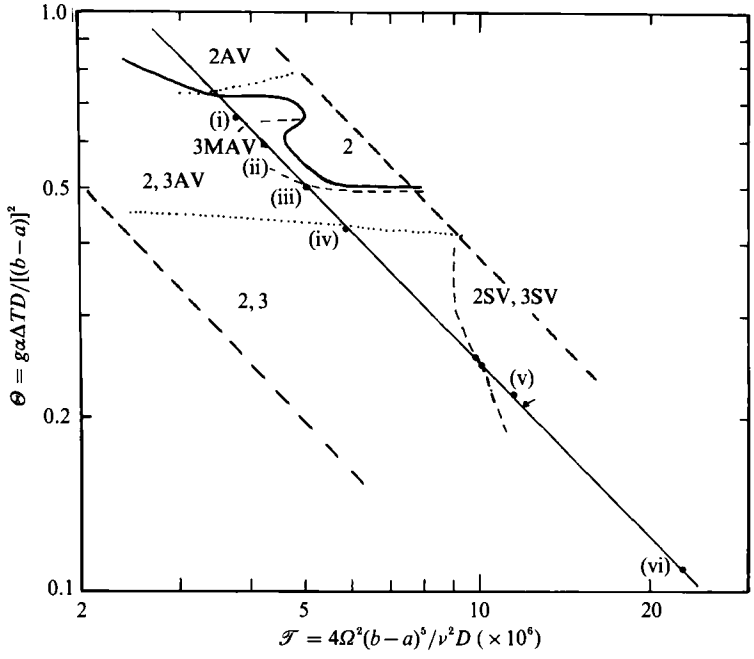

FIGURE 1. Regime diagram defining the regions of parameter space over which particular wavenumbers and flow types were observed. Numbers within each region denote the dominant azimuthal wavenumber m. Unqualified numbers denote a steady wave state, AV denotes amplitude vacillations, SV structural vacillations and MAV modulated amplitude vacillations (see text). The region explored is outlined by thin diagonal dashed lines, and the locus of $\Delta T = 10$ K is given by the solid diagonal line. Transitions between different wavenumbers are shown by solid curves, between regimes of the same wavenumber by heavy dashed curves, and the boundary between steady waves and AV by dotted lines. Representative cases discussed in the text are marked as points (i)–(vi).

An extensive study of the regime diagram as a function of rotation rate and temperature difference for the apparatus used here was carried out by HWCJS and H85, though for a fluid with a significantly lower Prandtl number ($Pr = 13.1$). The present work extends over a narrower range in Θ and $\mathscr{T}$ than in the work of HWCJS (the region explored in detail here is outlined by thick diagonal dashed lines in figure 1), and focuses on the transition sequences encountered in the region close to the line $\Delta T = 10$ K (indicated by the solid diagonal line in figure 1). The overall distribution of flow regimes found here is qualitatively similar to that found by HWCJS, but with some significant differences. The general locations of flow regimes are displaced with respect to HWCJS in the direction of lower Taylor number so that, for example, SV sets in at $\mathscr{T}$ as low as 10^7. The regime diagram obtained by H85 also showed the widespread incidence of multiple equilibria (see above), with the occurrence of regular AV flows in association with transitions to a lower wavenumber as Θ is increased (Ω decreased). As Pr is increased, it is generally found that AV becomes more widespread (e.g. Jonas 1981), and this trend is reflected in the regime diagram for the present system in figure 1 (in which dotted lines indicate the approximate locations of the $m = 3$–3AV and 2–2AV boundaries, arbitrarily defined following H85; see below), compared with that of H85 and HWCJS.

The boundary between $m = 3$AV and $m = 2$ was also found to be distorted from the monotonically increasing trend in Θ with $\mathscr{T}$ observed by HWCJS, owing to the development of a new regime for $\mathscr{T} > 3.5 \times 10^6$, designated $m = 3$MAV (i.e.

Case	Flow type	T (K)	Ω (rad/s)	Θ	$\mathscr{T}$ ($\times 10^6$)	τ_d (s)	$\tau_v(/\tau_m)$ (s)(/(s))	D_p	λ_1 ($\times 10^{-3}$ bit/s)
(i)	3AV	9.99	1.6263	0.659	3.76	543	175	2.18	0.51
(ii)	3MAV	10.01	1.7162	0.593	4.19	426	167/1310	2.97	1.79
(iii)	3AV	10.06	1.8730	0.500	4.99	544	143	2.18	0.19
(iv)	3	9.98	2.0302	0.422	5.86	651	133	1.20	0.24
(v)	3SV	9.98	2.8147	0.220	11.3	802	52	2.83	0.89
(vi)	3SV	9.97	4.0013	0.109	22.8	~ 1250	~ 60	3.36	4.76

TABLE 1. Experimental parameters

'modulated amplitude vacillation', for reasons discussed in §4 below). In the latter regime the modulation index of regular AV, η, defined by

$$\eta = (A_{\max} - A_{\min})/(A_{\max} + A_{\min}), \tag{3.3}$$

(where $A_{\max}$ and $A_{\min}$ are respectively the maximum and minimum wave amplitudes, cf. the quantity I_a of H85), began to vary irregularly on a relatively long timescale $\geqslant 1500$ s. At its peak, η became large (~ 1), so that the $m = 3$ pattern virtually disappeared at its minimum in the vacillation cycle. This transient increase in the strength of AV apparently caused the transition from $m = 3$ to $m = 2$ to occur more readily and at a lower value of Θ over the region in parameter space in which MAV occurred.

In order to examine the sequence of transitions in this region of parameter space in more detail, a number of long runs investigating $m = 3$ flows were carried out at $\Delta T = 10$ K (effectively at fixed Grashof number $Gr\,(=\Theta\mathscr{T}) = 6.19 \times 10^5$) and for various values of Ω (Taylor number $\mathscr{T}$). A representative cross-section comprising six of these runs is discussed below, designated cases (i)–(vi). The characteristics of these six cases are listed in table 1 and their parametric locations indicated along the $\Delta T = 10$ K line in figure 1. Cases (i) and (iii) are examples of periodic $m = 3$AV (though see §4.1 below concerning (i)), while a steady wave state is represented by case (iv). A typical MAV is illustrated by case (ii), and two cases of SV are represented by cases (v) (incipient SV) and (vi) (fully developed SV). In the following subsection we discuss the main features of these regimes, illustrated by examples selected from these six principal cases.

3.2. *Time series and spectra* (*figures* 2–4)

Figure 2 shows short (2500 s) segments of the raw temperature (T) and heat transport (N) data for representative cases of MAV, AV, steady waves and SV (cases (ii), (iii), (iv) and (v) respectively). In the steady wave (figure 2*c*), the temperature signal exhibits a simple periodic oscillation as the wave pattern drifts past the fixed measurement point, while the heat transport remains approximately constant (apart from a weak oscillation associated with a very weak residue of AV). In fully developed AV (figure 2*b*), the wave drift is still evident as a slow, regular oscillation in the temperature signal, but the (fast) modulation in amplitude is also evident and reflected in a strong periodic oscillation in total heat transport. This oscillation in total heat transfer itself becomes modulated in the MAV regime (figure 2*a*), resulting in a complex and rapidly varying temperature signal. The onset of SV, on the other hand, has a quite different signature (figure 2*d*). A weak and rapid, though irregularly fluctuating, component appears in the temperature signal, superimposed

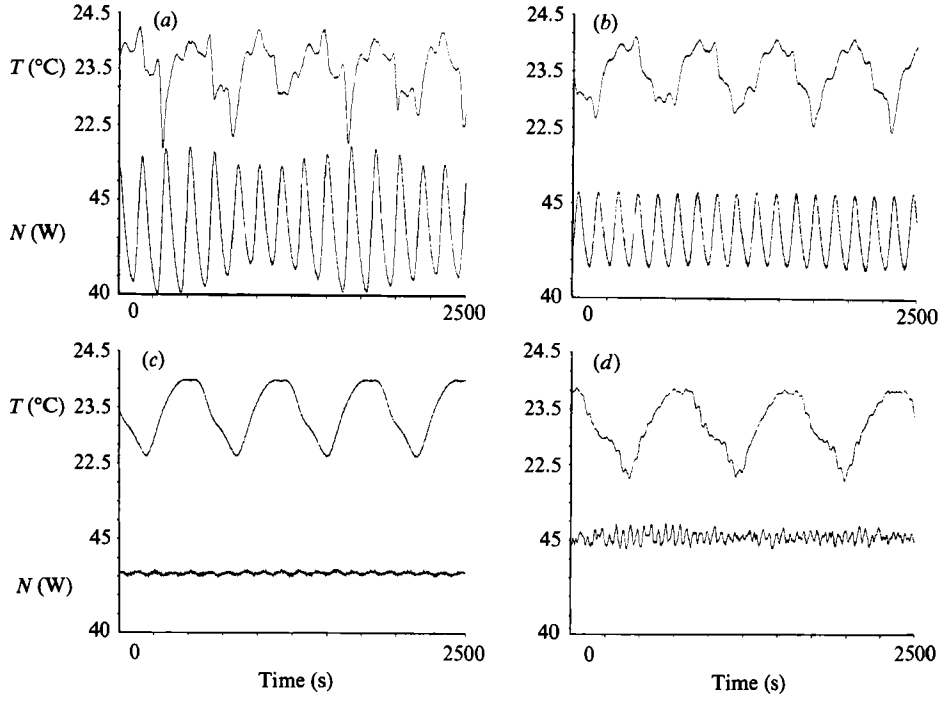

FIGURE 2. Extracts from time series of measurements of temperature T and total heat transport N for four representative flows with $m = 3$: (*a*) case (ii), (*b*) case (iii), (*c*) case (iv) and (*d*) case (v). Experimental conditions (Θ and $\mathscr{T}$) for each case are shown in table 1. Temperatures are in °C and heat transport is shown (approximately) in W.

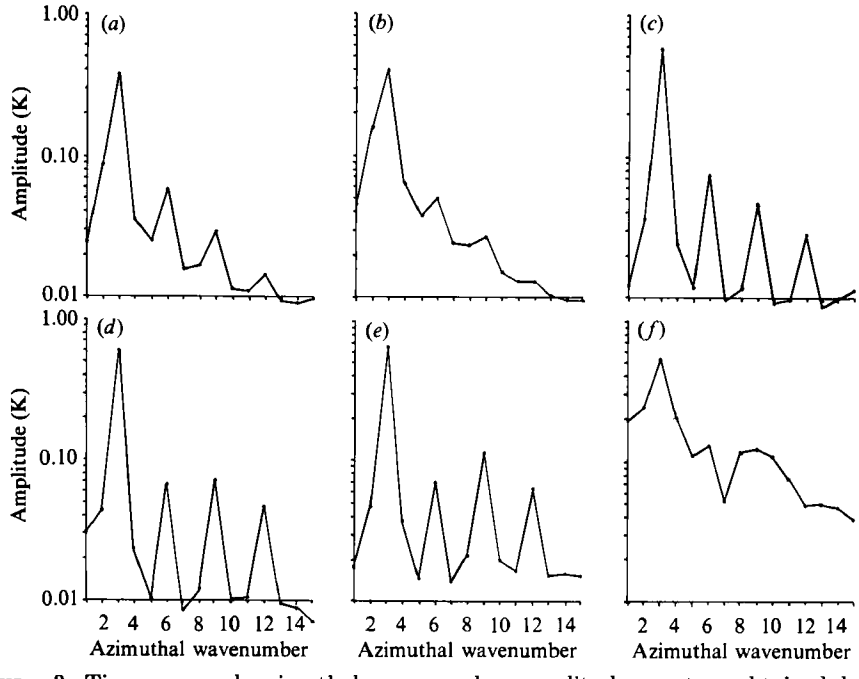

FIGURE 3. Time-averaged azimuthal wavenumber amplitude spectra, obtained by six representative flows: (*a*) case (i), (*b*) case (ii), (*c*) case (iii), (*d*) case (iv), (*e*) case (v) and (*f*) case (vi). Parameters for cases (i)–(vi) are shown in table 1.

upon the slow wave drift and accompanied by intermittent bursts of oscillation in total heat transfer.

The spatial and frequency spectra from all six principal cases are illustrated in figures 3 and 4. Figure 3 illustrates azimuthal wavenumber spectra from the 32-point thermocouple ring, averaged over several mean drift periods of the dominant wavenumber. The spatial spectra from two $m = 3$AV states (figure 3*a–c*) are dominated by the main wavenumber $m = 3$ and its harmonics. The amplitudes of the higher harmonics in cases (i)–(iv) increase with Ω until, in the steady wave regime (figure 3*d*), $m = 6$, 9 and 12 all become comparable (cf. H85). The sidebands of the dominant wavenumber are significantly non-zero, though for cases (iii)–(v) they are still smaller in amplitude than the harmonics (figure 3(*c–e*)). Analysis of the azimuthal phases showed that, at least for cases (i)–(iv), the sidebands ($m = 2$ and 4) have the same average frequency with respect to the apparatus as $m = 3$, but for cases (iii) and (iv) (see below), $m = 1$ was stationary, consistent with the forcing of $m = 1$ by small departures from axial symmetry in the apparatus and thermocouple ring (cf. Hide, Mason & Plumb 1977; James, Jonas & Farnell 1981). For cases (i) and (ii), the sidebands (especially the lower sideband) are significantly larger than harmonics $m = 9$ or 12, indicating the increasing presence of the $m = 2$ component as the transition from $m = 3$ to $m = 2$ is approached.

Figure 4 shows frequency power spectra from the time series at a single thermocouple (obtained by averaging individual spectra from each of five overlapping data segments of 16384 points spanning each run) (*a–c* and *g–i*), and power spectra of the inner cylinder heat flux (with the same spectral resolution, windows and sampling) (*d–f* and *j–l*). The temperature frequency spectra for cases (i) and (iv) (figure 4*a*, *g*) show the presence of strong components at the dominant wave drift frequency ω_d and its harmonics, the amplitude vacillation frequency ω_v and its harmonics, and a plethora of combination frequencies (cf. H85). The large number of discrete combination frequencies suggests that ω_v and ω_d are not commensurate, even for case (i) (for which $\omega_v \sim 3\omega_d$). This result is consistent, for example, with the findings of White & Koschmieder (1981), and would strongly suggest that frequency entrainment between ω_d and ω_v does not readily occur. Such a result would be expected on general grounds since, in the absence of departures from axial symmetry in the apparatus, no physical means of coupling the effects of wave drift and amplitude modulation exists. This kind of result was also predicted in the context of dynamical systems theory and symmetry arguments by Rand (1982).

For most of these flows, the total heat transport is also modulated as a result of the growth and decay of the waves during wave vacillation cycles (see figure 2). Frequency power spectra for the total heat transport are also shown in figure 4 which, for cases (i) and (iii), indicate a strong periodic modulation at ω_v and its harmonics (figure 4*d*, *f*). The index of modulation η (see (3.3)) shows a clear decrease towards zero with increasing Ω, almost disappearing into the steady wave state around case (iv) (see figure 4*j*). The drift frequency and some of its harmonics are also just detectable in the heat transport spectra, though of very small amplitude, arising presumably because of interactions with departures from axial symmetry due to imperfections in the apparatus and thermocouple array. In the case of (i), quite strong components at $\omega_v/3$ and $2\omega_v/3$ are also present (see §4.1 below).

The modulated amplitude vacillation regime (MAV) is illustrated in figures 3(*b*) and 4(*b*, *e*). Time-averaged spatial spectra in this regime are dominated by $m = 3$ and its harmonics, though non-harmonic components are also present at a much higher mean amplitude than for the regular $m = 3$AV flows (e.g. case (iii)). The temperature

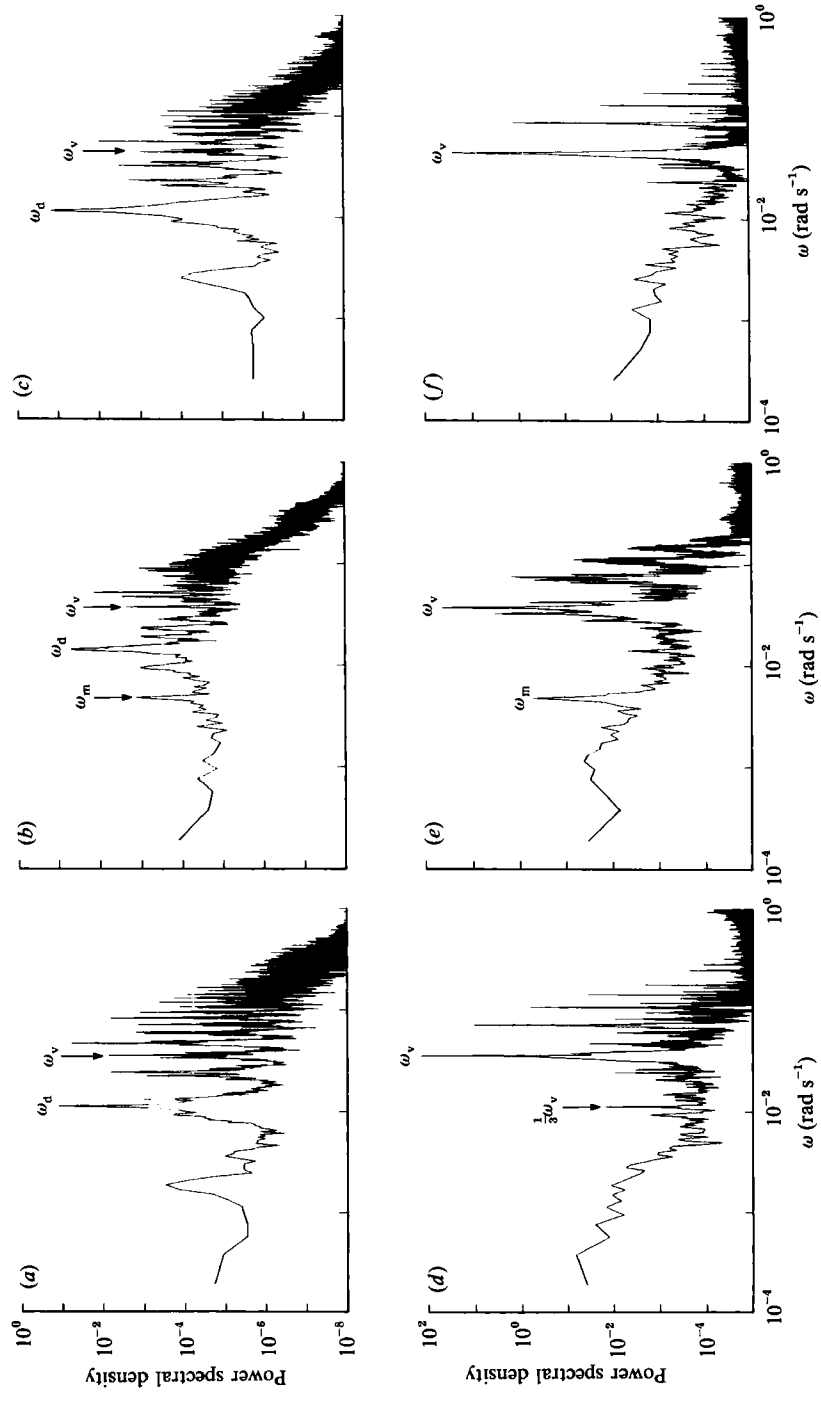
(a)
(b)
(c)
(d)
(e)
(f)
ω_d
ω_v
ω_m
$\frac{1}{3}\omega_v$
Power spectral density
ω (rad s^{-1})
10^0
10^{-2}
10^{-4}
10^{-6}
10^{-8}

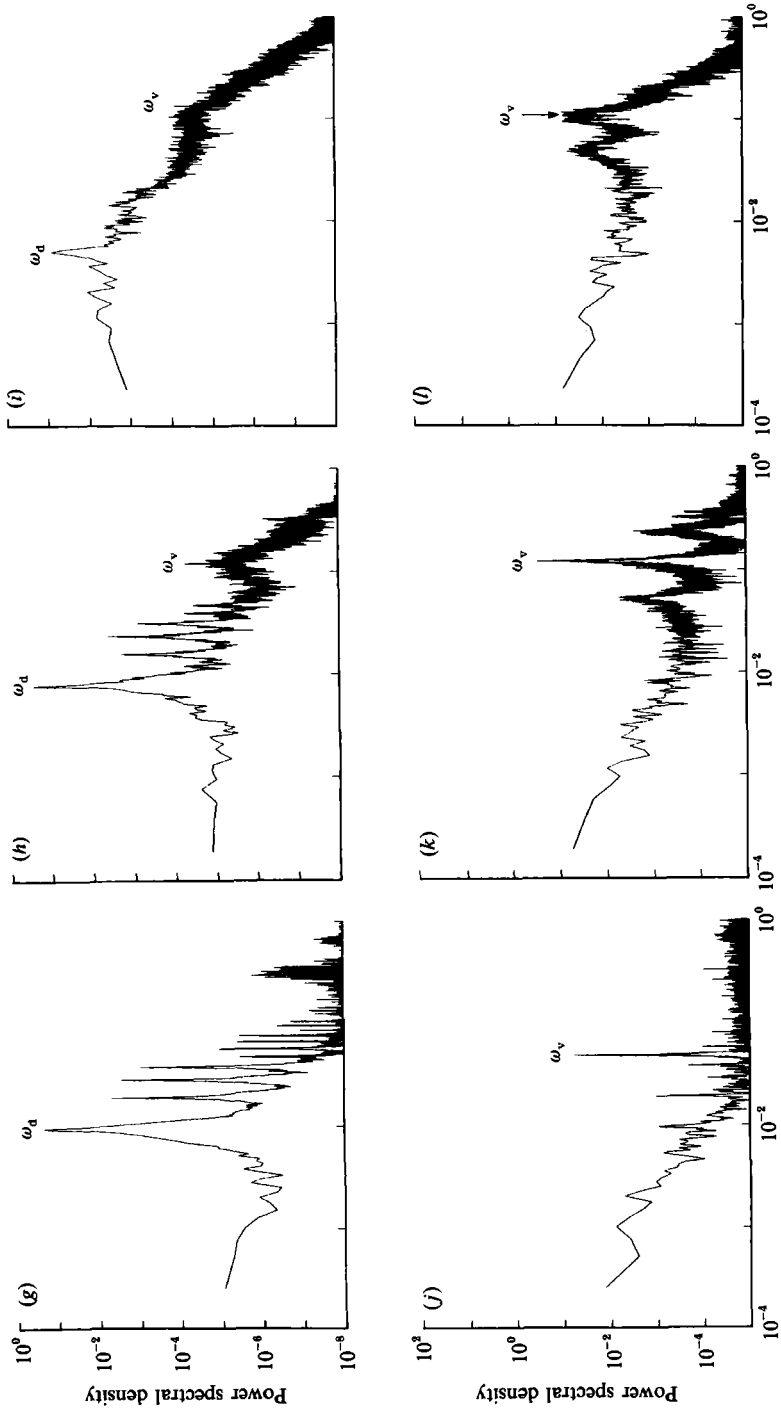

FIGURE 4. Frequency power spectra of temperature variations at a fixed location in the flow (mid-height and mid-radius) (*a–c*) and (*g–i*), and of total heat transport (*d–f*) and (*j–l*) for all six cases illustrated in figure 3: (*a–d*) case (i); (*b–e*) case (ii); (*c–f*) case (iii); (*g–j*) case (iv); (*h–k*) case (v); and (*i, l*) case (vi). Parameters for cases (i)–(vi) are shown in table 1.

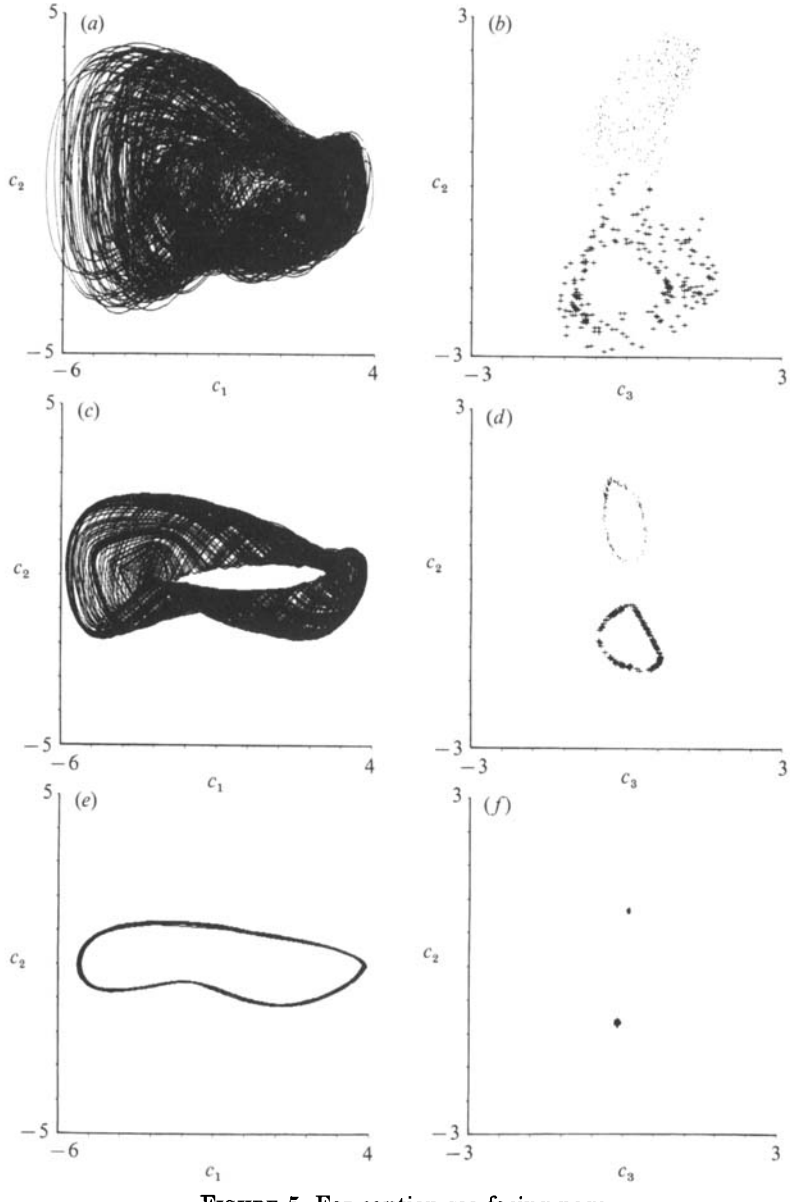

FIGURE 5. For caption see facing page.

frequency spectrum (figure 4*b*) shows rather fewer discrete components than in cases (i) and (iii), though peaks at ω_d, ω_v and their lower-order harmonics and combinations are present. Also present is a substantial broadband component extending to high frequencies. In the heat transport spectrum for case (ii) too (figure 4*e*), pronounced broadened peaks at ω_v and its harmonics are present, but with the additional presence of a new low-frequency component ω_m. Sum and difference components between ω_v and ω_m are also present, contributing to the broadening of the main peaks centred at $n\omega_v$ (n integer).

At intermediate Ω, the amplitude vacillation decays away until, by case (iv) (figures 2*c*, 3*d* and 4*g*, *j*), it is scarcely detectable. The resulting flows are quite well described as steady drifting waves. Spatial spectra are relatively clean and dominated

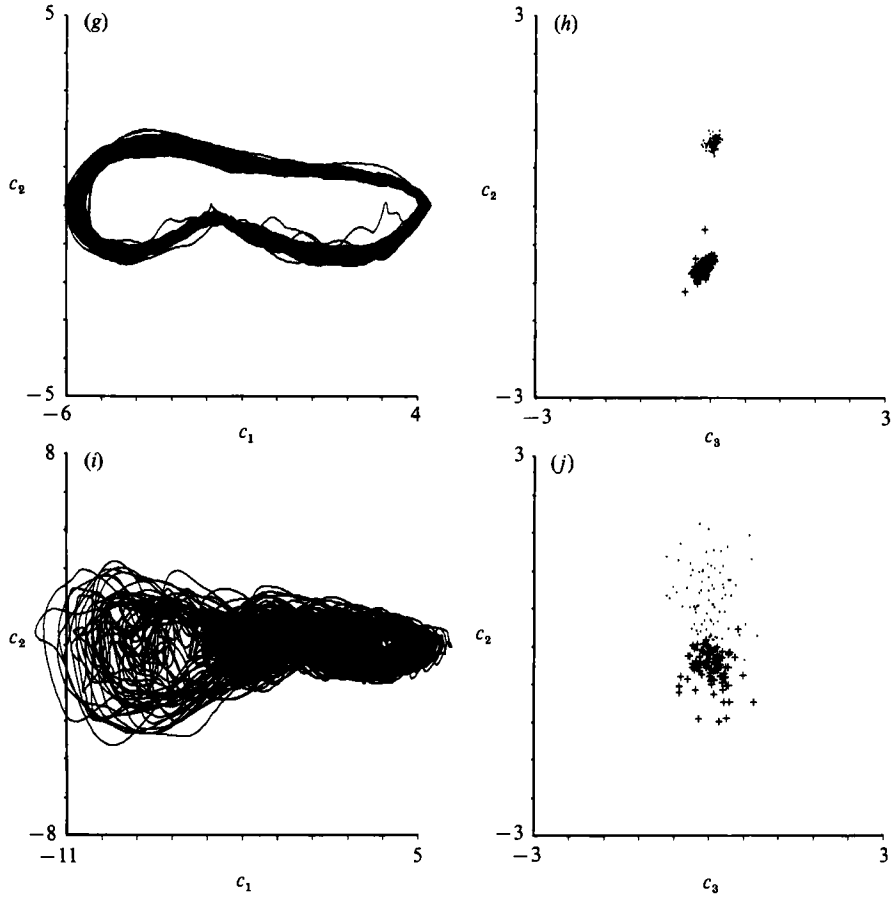

FIGURE 5. SVD phase portraits (*a*, *c*, *e*, *g* and *i*) and Poincaré sections (*b*, *d*, *f*, *h* and *j*) for five of the cases illustrated in figures 3 and 4, derived using a [50, 1] window on temperature time series from a single thermocouple in the flow: (*a*, *b*) case (ii); (*c*, *d*) case (iii); (*e*, *f*) case (iv); (*g*, *h*) case (v); (*i*, *j*) case (vi). Parameters for cases (ii)–(vi) are shown in table 1. Phase portraits are projected onto the first two singular vectors ($\boldsymbol{c}_1, \boldsymbol{c}_2$), and Poincaré sections are projected onto the ($\boldsymbol{c}_2, \boldsymbol{c}_3$) plane at $\boldsymbol{c}_1 = 0$. Dots denote positive-going sections (i.e. $\mathrm{d}c_1/\mathrm{d}t > 0$), crosses denote negative-going sections.

primarily by $m = 3$ and its harmonics, the latter being of comparatively large amplitude. The temperature frequency spectrum (figure 4*g*) is dominated by the main drift frequency ω_d and its harmonics, corresponding to the drift of the main wave and its spatial harmonics past the measurement point. Components corresponding to azimuthal wavenumbers up to at least $m = 33$ can be identified (corresponding to an azimuthal wavelength at mean radius of only 1.3 cm; e.g. see figure 4*g*). Also present, however, is a comb of weaker peaks between 0.25 and 0.4 rad s^{-1}, separated by ω_d, suggesting that one or more additional frequency components, incommensurate with ω_d and associated with another form of periodic behaviour, may be active. The presence of this set of components in T would seem to be associated with a weak but distinct component also present in the heat transport spectrum around 0.32 rad s^{-1}.

As Ω continues to increase through cases (v) and (vi), a form of structural vacillation sets in with a dominant frequency ω_v around 0.12 rad s^{-1}. The onset of SV initially has little effect on the mean azimuthal wavenumber spectrum. The frequency spectra, however, rapidly develop a number of broad peaks in both

temperature and heat flow between 0.1 and 0.3 rad s^{-1}. At the highest rotation rates (see case (vi)), SV has developed to the extent that, although the flow is still dominated by $m = 3$, even the main azimuthal harmonics are scarcely distinguishable from the non-harmonic components (cf. figure 3*f*). The temperature frequency spectrum shows only a single peak at the wave drift frequency (figure 4*i*), and otherwise resembles red noise, while the heat flow spectrum too (figure 4*l*) consists of broadband noise with broad peaks at 0.05 and 0.12 rad s^{-1}. The latter flow would therefore seem to lie in the 'transition zone' (in the terminology of Buzyna *et al.* 1984) prior to the development of fully irregular flow or geostrophic turbulence.

3.3. *Phase portraits* (*figures* 5 *and* 6)

Frequency and spatial spectra are clearly useful for characterizing temporally and/or spatially periodic flows, but convey only limited information on systems behaving aperiodically. In order to characterize the series of flows discussed above more fully, phase portraits of the single-location temperature and total heat transport time series were constructed using a version of Takens' 'method of delays' (Takens 1980). Takens' method was used for single-point time series only for practical reasons related to the limitations of the available data acquisition system (mainly on sampling rate and storage capability), though we recognize that a more satisfactory approach would be to use data taken simultaneously at several locations (cf. Guckenheimer & Buzyna 1983; Broomhead & King 1986). The SVD method was used to obtain optimum reprojections of the reconstructed trajectories, and a window length τ_w of between 75 and 100 s proved most suitable, given the relatively long wave drift periods. This value of τ_w is somewhat longer than would be suggested from the discussion of Broomhead & King (1986; their equation 3.20) though even $\tau_w = 100$ s is still less than most typical fundamental vacillation frequencies. Several other values of τ_w, both longer and shorter than 100 s, were also tried during the course of the analysis, down to $\tau_w = 20$ s, but the main results were found to be not significantly sensitive to τ_w provided it was not much longer than the shortest fundamental vacillation period.

Phase portraits from some of the examples discussed in §3.2 above are shown in figures 5 and 6, which show respectively results from the thermocouple time series and measurements of the heat transport. Trajectories are shown projected onto the first two eigenvectors ($\boldsymbol{c}_1$ and $\boldsymbol{c}_2$), and Poincaré sections consisting of intersections of the trajectory with the plane $\boldsymbol{c}_1 = 0$ are shown projected onto eigenvectors $\boldsymbol{c}_2$ and $\boldsymbol{c}_3$. For the two cases identified as quasi-periodic amplitude vacillations, (i) and (iii), thermocouple phase portraits lie on a 2-torus (see figure 5*c*, *d* for case iii), in which the main toroidal period represents the phase drift of the wave at ω_d and the poloidal oscillation represents the amplitude modulation at the vacillation frequency ω_v. The absence of any tendency for the trajectories to exhibit strong clumping in their Poincaré sections indicates that ω_d and ω_v are incommensurate, and confirms that these flows are indeed quasi-periodic.

Phase portraits from the heat transport time series for cases (i) and (iii) take the form of closed, near-circular loops of finite thickness, the orbital period of which corresponds to $2\pi/\omega_v$ (see figure 6*c*, *d* for case iii). The thickness of the trajectory, resulting in somewhat elongated clumps in the Poincaré sections, is consistent with slow instrumental drifts in the measurements, so that the trajectory apparently exhibits only the singly periodic behaviour associated with the amplitude vacillation. The heat transport time series therefore complements that of temperature by removing the component of the signal due only to the drift of an otherwise steady

flow pattern with respect to the apparatus (cf. the analyses of azimuthal mean flow by the use of an axial probe in the baroclinic two-layer open cylinder experiments of Hart 1985).

A case of MAV (ii) is shown in figures 5(*a*, *b*) and 6(*a*, *b*). The basic toroidal structure in the temperature phase portrait (figure 5*a*), similar to that of pure AV, is apparent but the Poincaré section (figure 5*b*) reveals that the 'walls' of the torus have a finite thickness significantly greater than can be accounted for by instrumental noise. Little systematic structure is apparent within the wall thickness itself, though the Poincaré section of figure 5(*b*) does contain some strand-like features in both branches. In the heat transport phase portraits (figure 6*a*), the wave drift component is again absent, and the trajectories appear to lie on a nearly disk-like structure of small though finite thickness. The thickness of the disk-like structure is comparable with or somewhat greater than that due to instrumental drift, though the intrinsic signal-to-noise ratio for the heat transport measurements is somewhat less than for the temperature time series. As shown in §4.1 below, the disk-like appearance belies the existence of a torus-like structure related to the two main frequencies ω_v and ω_m, which is not easily apparent in figure 6(*a*) because of the large mean 'winding number' $W(=\omega_v/\omega_m)$.

As the flow moves from amplitude vacillation into the steady wave regime (e.g. case iii), the toroidal structure of the temperature signal collapses onto a simple closed loop of very small thickness (see figure 5*e*). The decay of the strength of the vacillation is well represented in the heat transport phase portraits, in which the limit cycle appears to collapse almost to a point (apart from the effects of instrumental noise and parametric drift; see figure 6*d*).

The onset of SV in figures 5(*g*, *h*) and 6(*f*, *g*) initially has rather little effect on the temperature phase portrait, the weak vacillation resulting only in a slight thickening of the limit cycle beyond that due to instrumental noise. At the largest values of Ω, where structural vacillation is fully developed (case vi; see figure 5*i*, *j*), the limit-cycle structure is scarcely discernible in the temperature data. The phase portrait takes on a highly complex, rather ragged form with occasional excursions well beyond the confines of the original limit cycle in (iv) (associated with sporadic, strong and rapid cooling events in the time series). The heat transport phase portraits (e.g. figure 6*f*, *g*) show little systematic structure emerging with the onset of structural vacillation other than a broad separation of positive and negative passes; a more or less space-filling structure appears to emerge as soon as the structural vacillation reaches a perceptible amplitude. The phase portraits thus provide clear evidence of quite different qualitative behaviour between the onset of AV and SV.

3.4. *Dimensions and Lyapunov exponents* (*figure* 7)

In characterizing the behaviour of nonlinear systems, it is often desirable to detect the onset of chaotic behaviour in transitions from quasi-periodicity, and to obtain estimates of the degree of complexity of the flow. A variety of methods have appeared in the literature in recent years (e.g. see Eckmann & Ruelle 1985; Meyer-Kress 1986 for recent reviews). The most common method is to estimate the correlation dimension (Grassberger & Procaccia 1983) of the reconstructed attractor. This method is known, however, generally to require very large datasets which are densely sampled throughout the reconstructed attractor, the number of required points increasing exponentially with attractor dimension. Smith (1988), for example, concluded that the number of statistically independent points $N_{\min}$ required to estimate the correlation dimension to within $\pm 5\%$ of its true value exceeds 42^M,

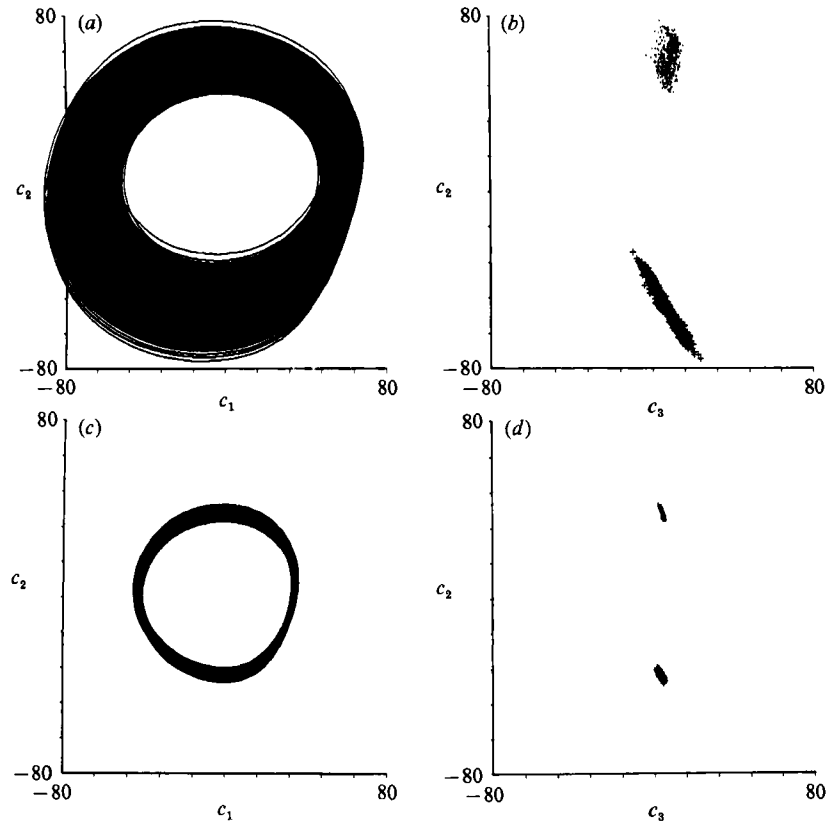

FIGURE 6. For caption see facing page.

where M is the greatest integer less than the dimension of the underlying attractor. With the present datasets ($N < 5 \times 10^4$), this would preclude the reliable estimate of dimensions significantly exceeding about 3. Even if sufficient data were available, the computational requirements for estimating the correlation exponent for flows other than the most simple would still be formidable.

The SVD method itself provides an estimate of the necessary embedding dimension of a dataset from the number of eigenvalues in the singular-value spectrum lying significantly above the 'noise floor' (cf. Broomhead & King 1986). This measure is not a robust estimate of the true dimensionality of the attractor, however, but depends on factors such as the local curvature of the underlying manifold (e.g. see Broomhead, Jones & King 1987), which in turn may depend upon the choice of sampling and window timescales τ_s and τ_w. Accordingly, we follow the approach suggested by Smith (1988) in using methods based on the analysis of localized regions of the reconstructed attractor. In the following analyses, we make use of the *locally defined* pointwise dimension D_p (Farmer, Ott & Yorke 1983) derived from the SVD phase portraits down to lengthscales limited only by the sampling and instrumental noise. For a given flow, the dimension quoted is an average over several (typically 20) randomly selected points across the reconstructed attractor. Some use was also made of the local SVD analysis of Broomhead *et al.* (1987) to provide additional verification of the values of D_p obtained.

Static invariants, such as the various dimension estimates discussed above, provided an indication of the overall intrinsic complexity of the behaviour of a

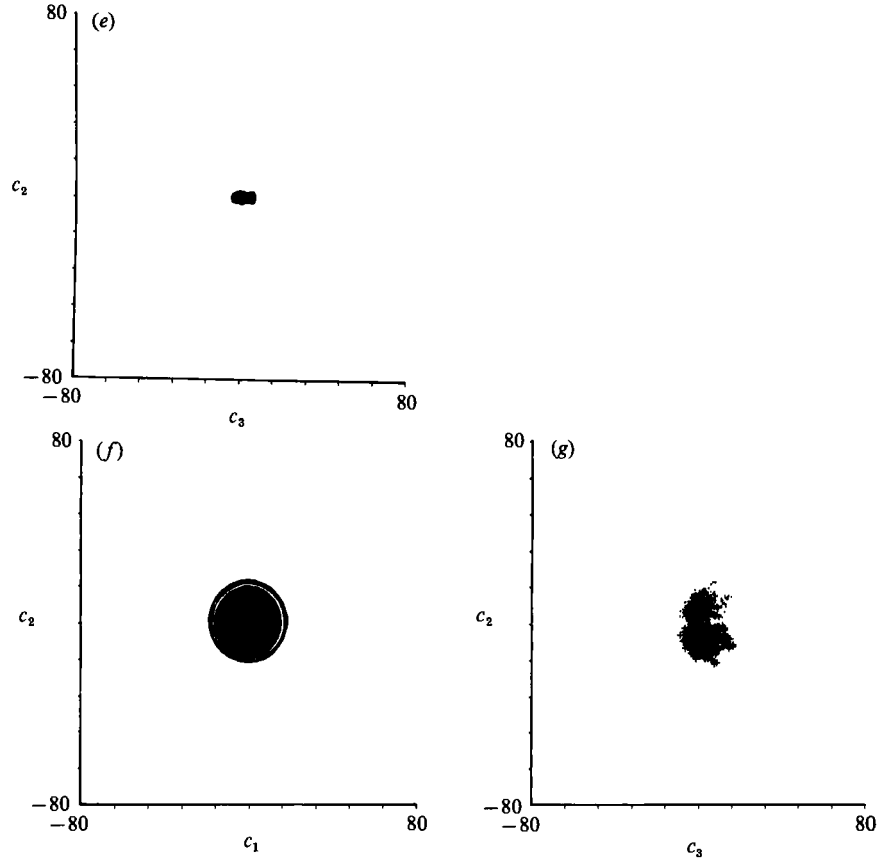

FIGURE 6. SVD phase portraits (*a*, *c*, *e* and *f*) and Poincaré sections (*b*, *d* and *g*) for four of the cases illustrated in figures 3–5, derived using a [50, 1] window on total heat transport time series: (*a*, *b*) case (ii); (*c*, *d*) case (iii); (*e*) case (iv), (*f*, *g*) case (v). Parameters for cases (ii)–(v) are shown in table 1. Phase portraits are projected onto the first two singular vectors (c_1, c_2), and Poincaré sections are projected onto the (c_2, c_3) plane at $c_1 = 0$. Dots denote positive-going sections and crosses denote negative-going sections.

dynamical system, but are not a particularly sensitive means of directly detecting the onset of chaos. Sensitive dependence on initial conditions is the critical property of chaotic behaviour, suggesting that an estimate of the largest non-negative Lyapunov exponent λ_1 would be the most suitable means of detecting the onset of chaos. In the present work, we use the algorithm suggested by Wolf *et al.* (1985), which directly measures the divergence of initially nearby segments of trajectories on the reconstructed attractor. Estimates of λ_1 were derived from attractors reconstructed using the simplest delay method as well as in SVD coordinates, with similar results being obtained. Consequently, results obtained from the SVD trajectories are presented below. As with the dimension calculations, the robustness of the results obtained was verified by repeating some of the calculations using a range of embedding dimensions ($5 < K < 12$), delay/window times ($20\text{ s} < \tau_w < 100\text{ s}$) and evolution timescales ($50\text{ s} < \tau_E < 700\text{ s}$; cf. Wolf *et al.* 1985).

Figure 7 shows estimates of (*a*) pointwise dimension D_p and (*b*) λ_1 for all the flows studied in the $Gr = 6.19 \times 10^5$ section as a function of Taylor number (the relevant values from temperature time series for cases i–vi are also shown in table 1). Solid

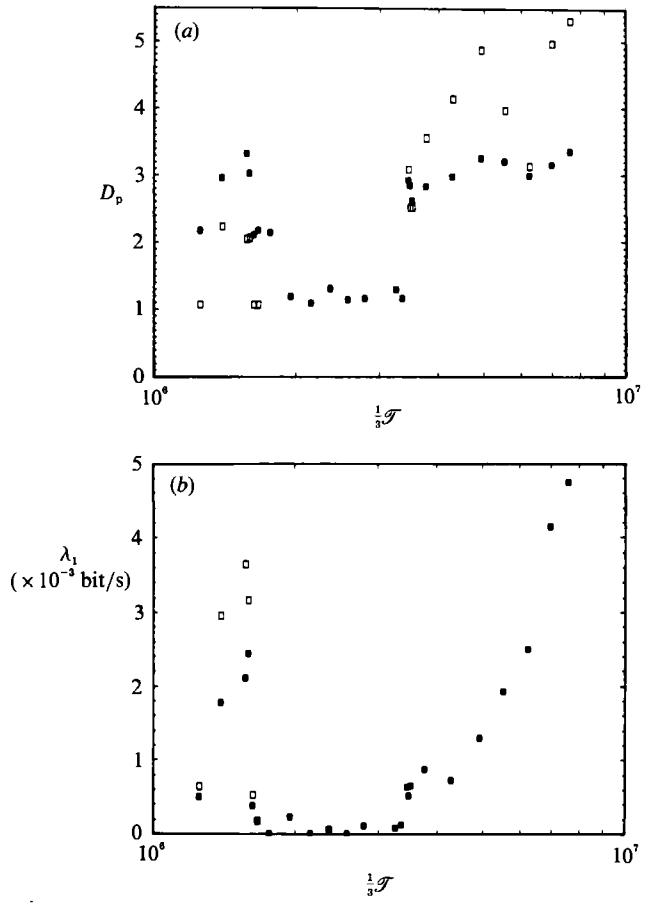

FIGURE 7. Estimates of (*a*) pointwise dimension D_p and (*b*) largest Lyapunov exponent λ_1, as a function of $\Omega(\mathscr{T})$ for $\Delta T = 10$ K. D_p was estimated using the method of Farmer *et al.* (1983), and λ_1 was estimated using the method of Wolf *et al.* (1985), both in SVD coordinates. Solid points denote temperature time series, and open squares denote total heat transport.

squares in figure 7 denote estimates derived from the temperature time series, and open symbols denote results for heat transport. Steady wave and regular AV flows consistently exhibit pointwise dimensions from the temperature datasets slightly exceeding 1.0 and 2.0 respectively, consistent with their respective appearance in the phase portraits (figure 5) as limit cycles and 2-tori. Pointwise dimensions for the AV cases were also calculated from the corresponding heat transport time series, and consistently resulted in $D_p \sim 1$, i.e. 1 less than that of the temperature dataset because of the absence of the component due to the wave drift. The largest Lyapunov exponent associated with these flows is consistently indistinguishable from zero, with an upper limit for λ_1 of around 4×10^{-4} bits s^{-1} (implying an intrinsic 'error-doubling' time of > 2500 s or ~ 1200 'days', corresponding to $\lambda_1 \leqslant 0.2$ bits per orbit).

Sharp boundaries between quasi-periodic and apparently chaotic behaviour are found at Taylor numbers of 4.8×10^6 and 1.0×10^7 (and also probably at 3.8×10^6), associated with the transitions from regular flows respectively to MAV and SV. On crossing the boundary from a quasi-periodic regime, D_p jumps to a value around 3 and λ_1 becomes significantly positive. In the case of the $m = 3$MAV flows, there is a very sharp transition at $\mathscr{T} = 4.8 \times 10^6$ to a state with $D_p \sim 3.2$, and

$\lambda_1 \sim 2.0 \times 10^{-3}$ bits s^{-1} (~ 1 bit per orbit), with little variation in these estimates across the MAV regime. The heat transport datasets also indicate a sharp transition to chaotic behaviour at this point, with D_p jumping to around 2 and λ_1 consistent with the temperature data (around 3×10^{-3} bits s^{-1}).

At the transition to structural vacillation at $\mathscr{T} = 1.0 \times 10^7$, λ_1 becomes significantly positive at a well-defined value of $\mathscr{T}$. The estimate of λ_1 is initially quite small, then increases rapidly with Taylor number. The pointwise dimension for $T(t)$ in this regime, however, remains close to 3, though with some evidence for a gradual increase in D_p with increasing $\mathscr{T}$. Some attempts were also made to estimate D_p from heat transport datasets in this regime though, in contrast to the MAV regime, the results do not indicate consistency with $T(t)$. In particular, estimates of D_p from $N(t)$ consistently equal or exceed those from $T(t)$, suggesting either that the estimates in this regime are in error or that the flows are not adequately characterizable as low-dimensional attractors. Evidence for extensive scaling regions in the correlation functions obtained in this regime was often found to be marginal, with scaling behaviour often present only over a fraction of a decade in relative radius. Neither of the two possibilities raised above can therefore be ruled out (see §5.1 for further discussion).

We have therefore identified two distinct regions of parameter space at which a periodic (or quasi-periodic) flow gives way to an apparently chaotic state with finite predictability and (at least for the MAV regime) a small attractor dimension ($D_p \leqslant 3.5$). The detailed properties of these two chaotic regimes appear to be quite different, however, and the following section discusses these properties and the transitions leading to their development in greater depth.

4. Quasi-periodic and chaotic regimes

4.1. *Periodic and chaotic amplitude vacillation*

The observed characteristics of periodic amplitude vacillation have been described in some detail by Pfeffer *et al.* (1980), HWCJS, H85 and Buzyna *et al.* (1989). Amplitude vacillation is generally observed to be a quasi-periodic phenomenon in which the dominant azimuthal wavenumber and its harmonics are periodically modulated in both amplitude and frequency (or phase speed) with a period $\sim$30–100 times that of the background rotation $\tau_0 (= 2\pi/\Omega)$. The dominant wavenumber exhibits a periodic growth and decay, with relatively rapid growth and a slower rate of decay (cf. H85, though contrast Buzyna *et al.* 1989). As discussed above, the total heat transfer is also modulated at the vacillation frequency, but with a small phase lag with respect to the dominant wavenumber, such that maximum heat transfer occurs just as the amplitude of the dominant wavenumber begins to decay.

At the onset of the MAV regime, slow irregular oscillations were found to occur in the modulation index of the total heat transfer and amplitude of the dominant wavenumber and its harmonics, apparently leading to a chaotic attractor organized about a 2-torus in temperature variations (e.g. figure 5*a*), but with more complex, apparently disk-like structure in heat transport (e.g. figure 6*a*). An indication that there may be more structure to the flow than figure 6(*a*, *b*) would suggest is evident from figure 8(*a*, *b*) which show the Poincaré section from figure 6(*a*) and the return map obtained by plotting $c_2(n)$ against $c_2(n+1)$ for each successive crossing by the heat transport trajectory of the plane $c_1 = 0$ (in the sense of c_1 decreasing).

The method of delays (and SVD) can produce very poor embeddings of flows with two widely separated dominant frequencies, particularly when the time delay (or window length in the case of SVD) is chosen to suit the higher frequency. This point

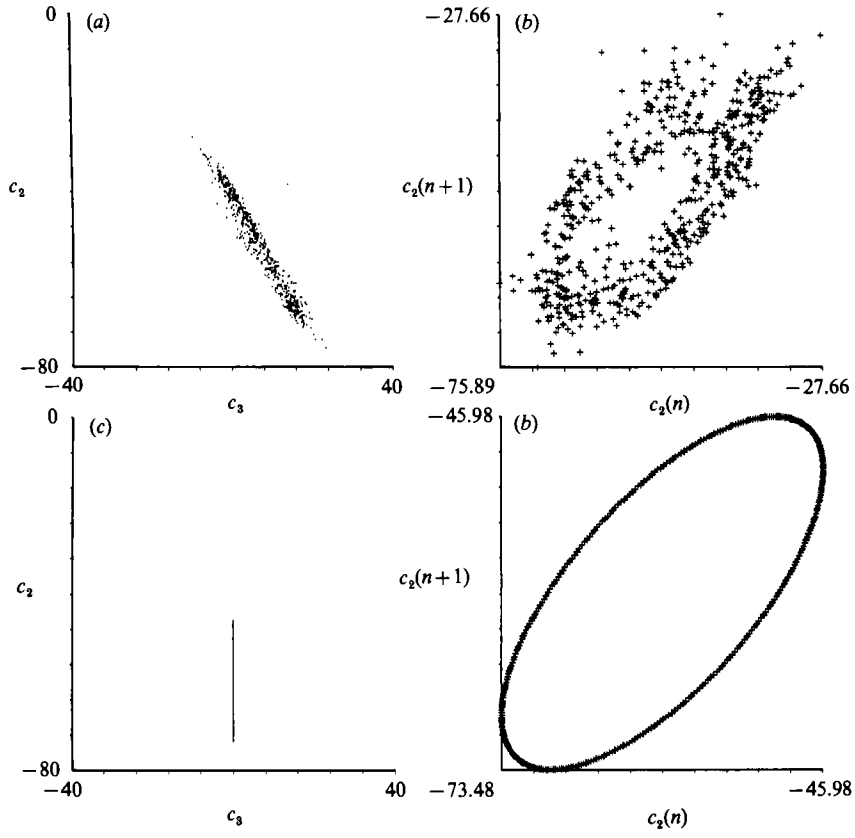

FIGURE 8. (*a*) Negative-going Poincaré section and (*b*) first return map, obtained by plotting successive values of c_2 from the Poincaré section in (*a*), for the time variation of heat transport from the $m = 3$MAV flow (case ii); (*c*) negative-going Poincaré section and (*d*) first return map ($c_2(n)$, $c_2(n+1)$) from the phase portrait obtained from the artificial quasi-periodic time series $A(t) = A_0 + (A_1 + A_2 \sin \omega_2 t) \sin \omega_1 t$. Series in (*c*) and (*d*) were sampled every 2 s, with $A_0 = 185$, $A_1 = 13$, $A_2 = 3$, $2\pi/\omega_1 = 167.0$ s and $2\pi/\omega_2 = 1310$ s, and analysed using $\tau_w = 100$ s.

is illustrated in figure 8(*c*, *d*) using an artificial quasi-periodic time series generated from

$$A(t) = A_0 + [A_1 + A_2 \sin \omega_1 t] \sin \omega_2 t, \tag{4.1}$$

with $\omega_1 \ll \omega_2$, and analysed using a SVD window based on the shorter period τ_2. The amplitudes, frequencies and window length used in (4.1) and figure 8(*c*, *d*) were chosen so that the signal approximately simulates case (ii) in figure 6(*a*, *b*) (see caption to figure 8 and table 1 for details). Because $\omega_1 \ll \omega_2$, the Poincaré section from the artificial time series in figure 8(*c*) nearly collapses onto a line parallel with the c_2 axis, and the return map (figure 8*d*) comprises a perfect ellipse with its major axis aligned along $y = x$ (cf. the 3MAV return map of figure 8*b*). A better embedding of the flow in three dimensions can be achieved by regarding the coefficients $c_1(t), c_2(t), c_3(t) \ldots$ as the basic observables and taking the coordinates of the embedding to be $(c_1(t), c_2(t), c_2(t+\tau))$. Results close to optimum are obtained when τ is chosen to be roughly equal to one-quarter of the period of the lower frequency (i.e. $2\pi/\omega_1$).

Figure 9(*a*) presents the negative-going Poincaré section at $c_1 = 0$ in the $(c_2(t), c_2(t+\tau))$ plane for case (ii) (that chosen for figure 8*a*, *b*) using $\tau \approx \frac{1}{4}\tau_m$. Its appearance is very similar to that of figure 8(*b*), though is more closely circular. Note that, if τ were chosen to be close to the shorter of the dominant periods (i.e. τ_v), the Poincaré

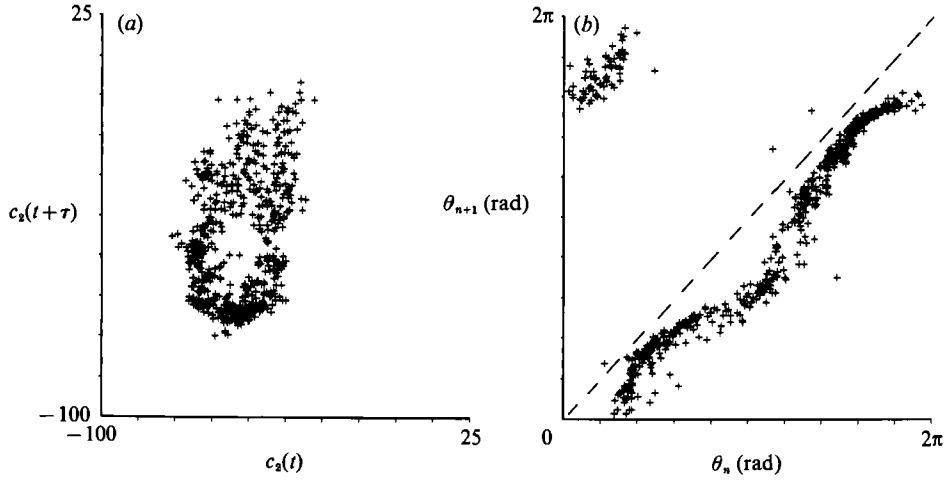

FIGURE 9. (*a*) Poincaré section (at $c_1 = 0$) in the $[c_2(t), c_2(t+\tau)]$ plane with $\tau = 350$ s ($\approx \frac{1}{4}\tau_m$) for the time variation of heat transport from an $m = 3$MAV flow (case ii), and (*b*) first return circle map, obtained by plotting successive values of azimuth angle θ about the centre of mass of (*a*).

section would be almost identical to the return map of figure 8(*b*). As anticipated, figure 9(*a*) provides a section consisting of points scattered about a closed loop, confirming the presence of toroidal structure in the heat transport signal. Taking the centre of mass of the points as the origin, the points on the section can be specified by polar coordinates (r, θ), in which the angle θ effectively represents the phase of the modulation frequency. Figure 9(*b*) displays the quasi-circle return map $(\theta(n), \theta(n+1))$. Clearly the phase of the modulation increases progressively, in agreement with the heuristic description (by analogy with (4.1)) of the modulation as quasi-periodic, but in two regions the map approaches the diagonal (on which $\theta(n) = \theta(n+1)$). Since points progress slowly through these regions, a large fraction of the points are clustered about them. Where the map approaches the diagonal, its shape would appear to be similar to that on which the type I intermittency route to chaos is based (e.g. see Bergé, Pomeau & Vidal 1984). It is important to remark, however, that the precise shape of the return map is quitely strongly sensitive to the choice of embedding parameters (especially τ), and the wavy and inhomogeneous nature of figure 9(*b*) appears to be largely due to the ellipticity of the Poincaré section in figure 9(*a*). It is reasonably clear, however, that the return map shows no obvious evidence for any non-invertible region, although the noise level is such that a small region of non-invertibility cannot be ruled out.

From the above discussion, we may infer that the flow in the 3MAV regime is largely deterministic. $T(t)$ is apparently organized about a 3-torus with incommensurate frequency components centred at ω_d, ω_v and ω_m. A pure 3-torus flow would not, however, be chaotic (an application of the Wolf *et al.* 1985 algorithm to the time series in (4.1) and figure 8*c*, *d*, for example, led to $\lambda_1 \approx 0$). In contrast, all other evidence relating to the 3MAV flows in figures 5–7 appears to point to chaotic behaviour, implying that an additional aperiodic component is also present, possibly accounting for much of the irregular radial scatter in figures 8(*b*) and 9(*a*). Whether the nature of this aperiodic component is due either to deterministic chaos or to quasi-stochastic perturbations, remains somewhat uncertain (see §5.3).

Upon closer examination of the spatial structure of the 3MAV flows, it was apparent that the spectrum of wavenumbers participating in the MAV is significantly

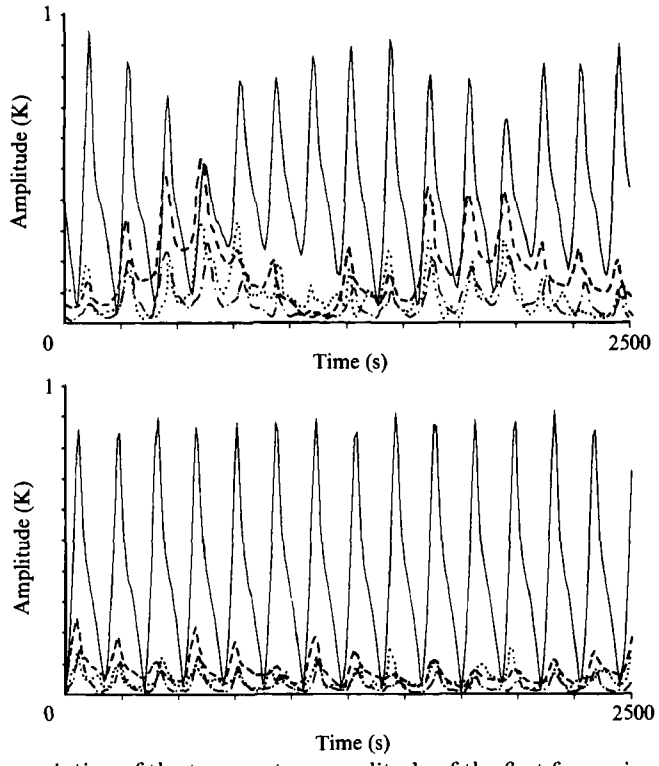

FIGURE 10. Time variation of the temperature amplitude of the first four azimuthal Fourier modes at mid-height and mid-radius in (*a*) a chaotically modulated $m = 3$MAV (case ii) and (*b*) the large-η $m = 3$AV (case i): ——, $m = 3$; – – –, $m = 2$; —·—·—, $m = 4$; ·····, $m = 1$ ($\times 2$).

more complicated than for straightforward periodic AV. Figure 10(*a*) shows the typical evolution of the amplitudes of wavenumbers $m = 1$–4 at mid-height and mid-radius, showing just over one period of the long-timescale modulation ($\tau_m \sim 2000$ s). All components are evidently vacillating at the same frequency, but with the long-period modulation of $m = 3$ almost in antiphase with that of $m = 2$. Indeed around $t = 700$ s, $m = 2$ almost achieves dominance over $m = 3$, though this is very short-lived.

The apparent coherence of the amplitude fluctuations of $m = 2$–4 (and $m = 1$?) is further confirmed from their respective phase propagation. All three wavenumber components $m = 2$–4 were found to drift at approximately the same frequency, such that the 'phase-locking function' (as suggested by Hide, Mason & Plumb 1977, and James *et al.* 1981), defined by

$$\Phi_m = \phi_{m+1} + \phi_{m-1} - 2\phi_m \tag{4.2}$$

(where ϕ_m is the instantaneous azimuthal phase of wavenumber m), was approximately constant for $m = 3$ at $\Phi_3 = \pi$ (see figure 11, where Φ_3 has only been calculated when the amplitude of all three components was greater than 0.06 K to ensure adequate signal-to-noise ratio). At the same time, $m = 1$ was found to drift slowly in relative phase with respect to the apparatus, with a frequency roughly similar to ω_m. On closer examination, however, it was apparent (e.g. from plots of Φ_2) that $m = 1$ was not phase-coherent with $m = 2$–4. Because $m = 1$ is consistently smaller in amplitude than the other three lowest wavenumbers, quantities such as Φ_2 can only be reliably calculated more sparsely than for Φ_3. Nonetheless, it is found

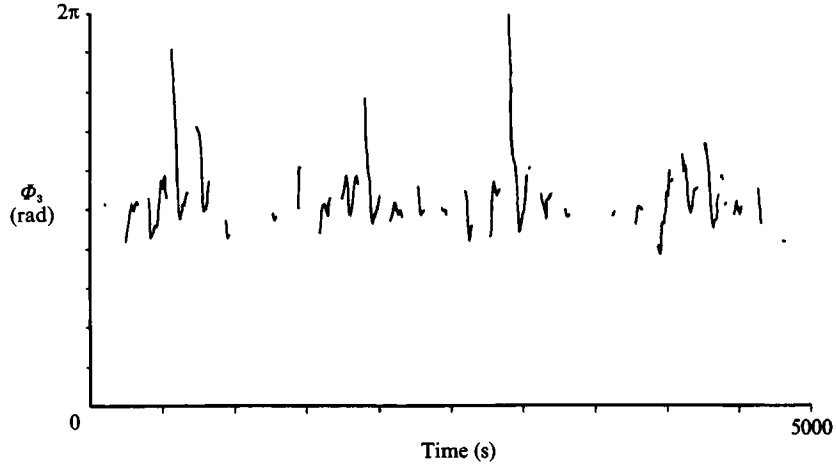

FIGURE 11. Time variation of the phase-locking function Φ_3 (see text and (4.2)) for a chaotic $m = 3$MAV flow (case ii). The function is plotted only where the temperature amplitude of all three wavenumber components exceeds 0.06 K.

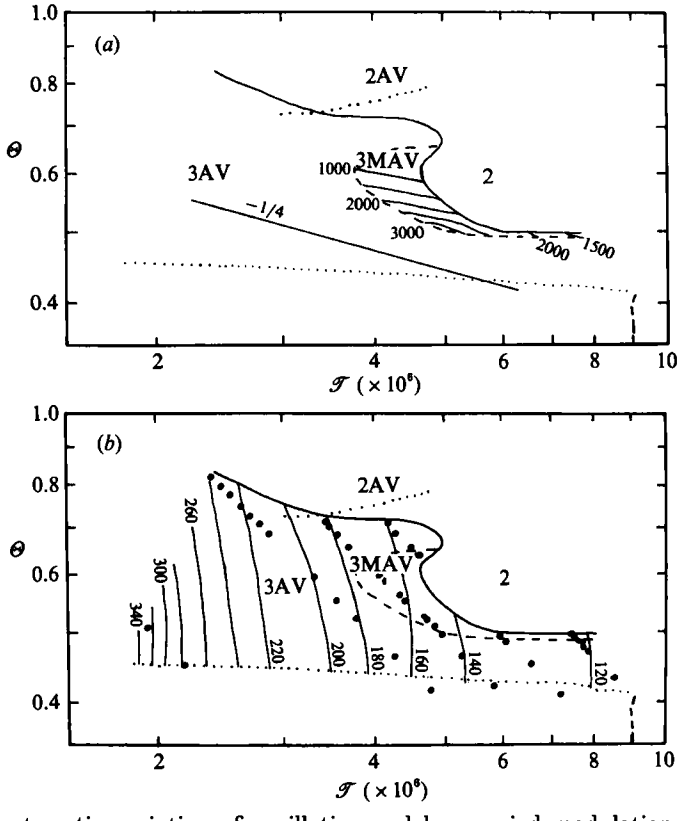

FIGURE 12. Systematic variation of vacillation and long-period modulation periods (τ_v and τ_m respectively) with external parameters, obtained from experimental measurements: (*a*) subjectively interpolated contours of τ_m in the $m = 3$MAV regime, (*b*) contours of τ_v in the $m = 3$AV and MAV regimes. Contour intervals are (*a*) 500 s and (*b*) 20 s, and selected contours are labelled with the absolute period in s.

that Φ_2 is much more variable than Φ_3, taking values over the full range 0–2π with apparently uniform probability.

This would suggest that the most obvious path for wave–wave interactions in a sideband instability (i.e. involving a pair of resonant triads, each of which includes $m = 3$, its upper or lower azimuthal sideband and $m = 1$), is not active in this flow. James *et al.* (1981) also found that this set of triad interactions was not active in the regular wave regime of the annulus. They pointed to an alternative route, found in their numerical simulations to result in the excitation of sidebands, via the first harmonic of the dominant wavenumber (i.e. triads involving (*a*) the self-interaction of $m = 3$ to excite the harmonic $m = 6$, and (*b*) $m = 6$ losing energy to $m = 4$ and 2; see James *et al.* 1981, their figure 7), which would also be consistent with a constant value for Φ_3 without involving the long wave $m = 1$. This route may thus help to excite a form of modal competition between adjacent wavenumbers, giving rise to temporal chaos, though with a strong degree of spatial order as observed.

The vacillation frequency is found to vary systematically in parameter space, such that ω_v is primarily dependent on $\mathscr{T}$ (see figure 12*b*), and is apparently a continuously increasing function of $\mathscr{T}$, even within the MAV regime. Regression analysis indicates that $\tau_v \sim \mathscr{T}^{-0.62}$ to a good approximation (see figure 13*b*). Figure 12(*a*) shows (subjectively interpolated) contours of τ_m as measured within the $m = 3$MAV regime, indicating that the modulation period reduces rapidly as Θ is increased. The contours of τ_m appear roughly parallel with the line $\Theta\mathscr{T}^{\frac{1}{4}} =$ constant ($\sim 1/R$, where R is the 'dissipation parameter' $R = E^{\frac{1}{2}}/Ro$, E being the Ekman number and Ro the Rossby number; cf. Pedlosky 1970; Hart 1986). Regression analysis of the observed variation suggests that $\tau_m \sim R^{8.7}$ (see figure 13*a*), indicating a considerable sensitivity of ω_m to Θ, and suggesting that $W = \omega_v/\omega_m \sim \Theta^{-8.7}\mathscr{T}^{-1.6}$.

As Θ is increased through the MAV regime, it was noted in §3 that a large-amplitude periodic AV regime was apparently recovered for a small interval in Θ before $m = 3$ gave way to a weak $m = 2$AV around $\Theta = 0.75$ (see figure 1). Upon close examination of the time variation of each individual azimuthal wavenumber component within the large-amplitude 3AV regime, it is evident (figure 10*b*) that, as in the 3MAV state, the sidebands of the dominant wave have significant amplitude and vacillate in phase with $m = 3$ with a near-constant value of the phase-locking function Φ_3. Furthermore, the peaks in the amplitudes of $m = 2$ and 4 are not uniformly similar, but undergo a roughly cyclic variation with a period close to $3\tau_v$. This period-3 modulation would seem to be an extension of the long-period modulation which forms part of the chaotic 3MAV regime, since the frequency ratio $W = \omega_v/\omega_m$ is found to vary systematically with Θ (and, to a much lesser extent, with $\mathscr{T}$).

We therefore conclude that the case (i) $m = 3$AV flow is simply a state within the 3MAV regime, but in which ω_v and ω_m are phase-locked in the ratio 3:1, reducing the effective number of independent frequencies in the flow to two (i.e. ω_d and ω_v). Hence the flow is quasi-periodic rather than a chaotic vacillation. The azimuthal components $m = 2$–4 are again found to have approximately the same average frequency, and the two modes of amplitude oscillation are presumably phase-locked through the same nonlinear interactions as responsible for the chaotic $m = 3$MAV states as discussed above.

4.2. *'Steady' waves*

The existence of a regime simply comprising a single dominant wavenumber component and its harmonics, which drift steadily at constant amplitude, has been a matter of controversy for several years. Hide & Mason (1975) and HWCJS indicate

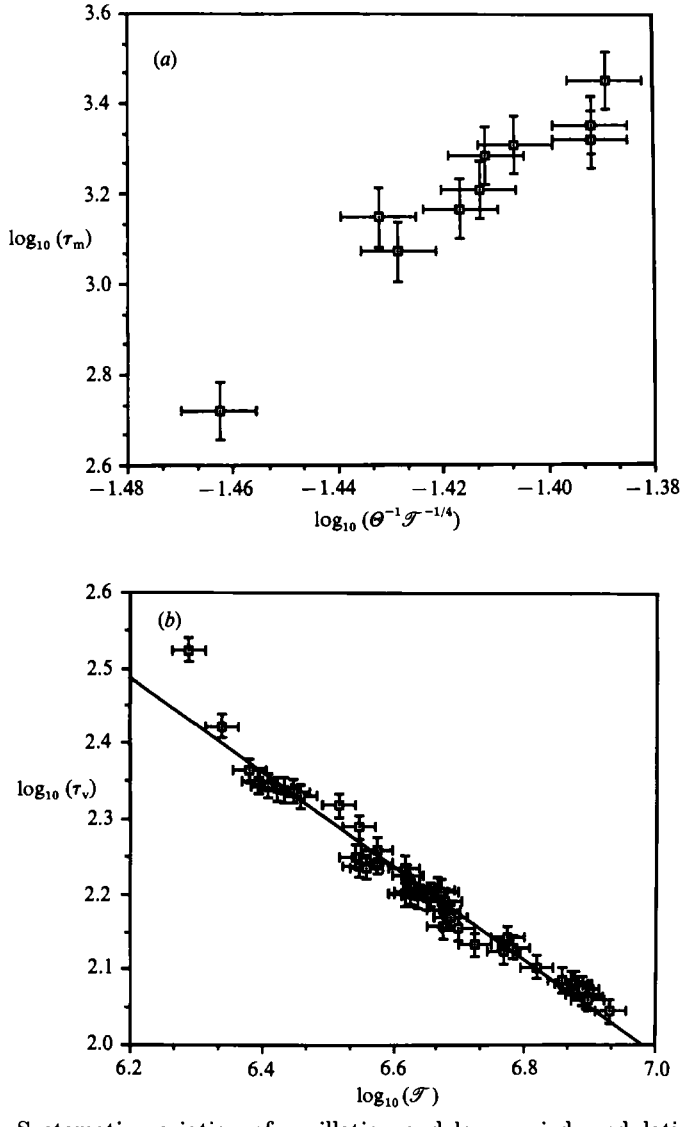

FIGURE 13. Systematic variation of vacillation and long-period modulation periods (τ_v and τ_m respectively) with external parameters, obtained from experimental measurements and plotted logarithmically: (*a*) τ_m *vs.* $\Theta^{-1}\mathcal{T}^{-1/4}$; (*b*) τ_v *vs.* $\mathcal{T}$.

the existence of such a regime in a region of parameter space intermediate between the AV and SV states, while Pfeffer *et al.* (1980) and Buzyna *et al.* (1984) report a direct transition between AV and SV and do not observe any steady waves. The source of this controversy might be due in part to a matter of definition (H85, for example, defines AV as a state in which $I_a \geqslant 0.05$, corresponding here to $\eta \geqslant 0.07$). In the present study, the amplitude of AV is found to decrease uniformly towards zero as Ω increases. Thus, case (iii) in figures 2–6 marginally qualifies as a steady wave state under the terms of H85's definition. Nevertheless, it is clear from the frequency spectra of heat transport that a weak oscillation at a frequency continuously traceable from ω_v in case (i) is present right into the SV regime.

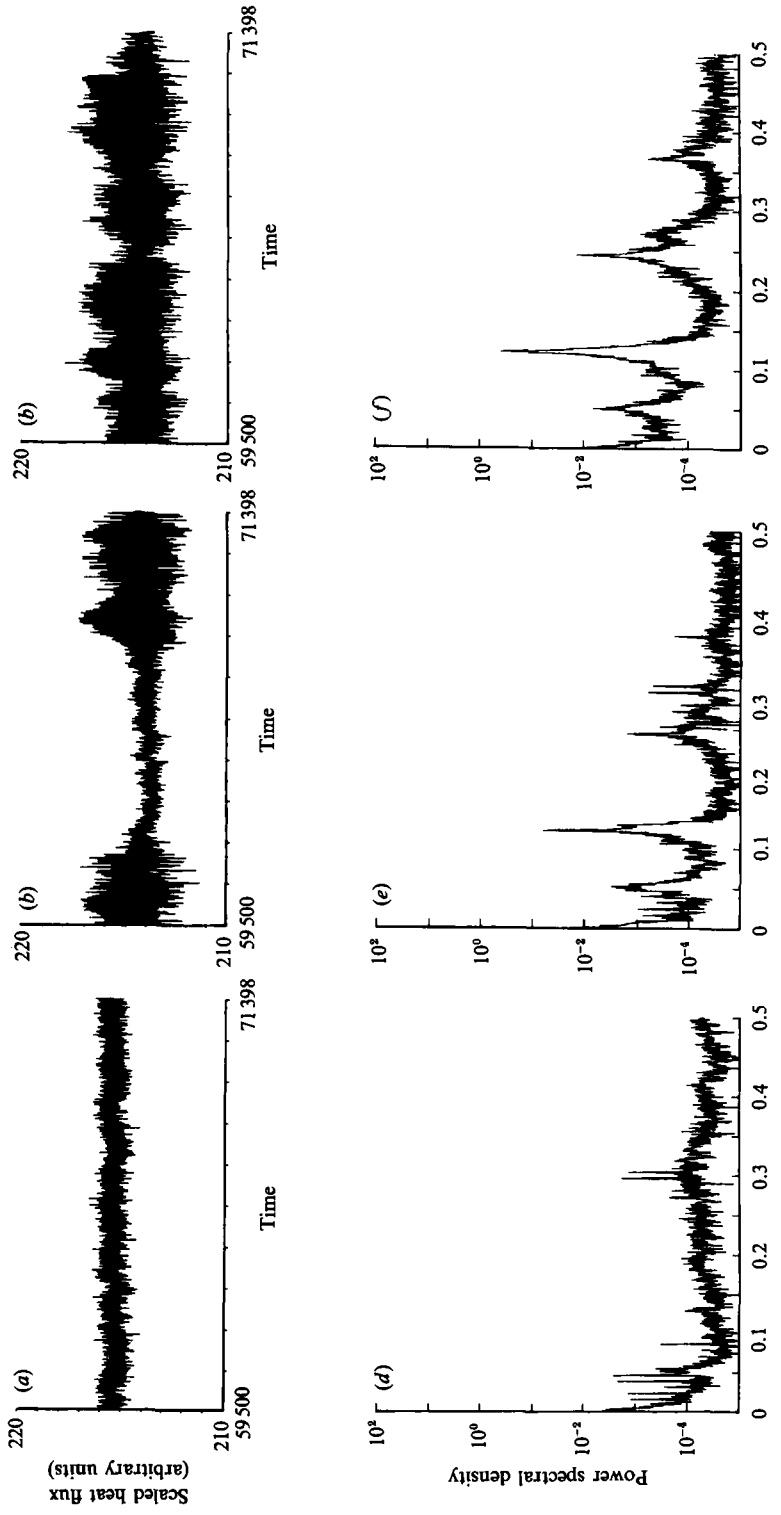

FIGURE 14. Extracts from (*a–c*) time series and (*d–f*) power spectra of total heat transfer from three flows close to the onset of chaotic structural vacillation (3SV). $\Theta \sim 0.25$, and (*a*, *d*) $\mathscr{T} = 9.81 \times 10^6$; (*b*, *e*) 9.84×10^6 and (*c*, *f*) 9.86×10^6.

4.3. *Structural vacillation*

The spatial and temporal characteristics of SV have been discussed from different viewpoints by Hide & Mason (1975), Pfeffer *et al.* (1980) and Buzyna *et al.* (1984). All these authors identify wave shape or structural vacillation with a roughly periodic variation in the shape or orientation of the dominant wave, but with relatively small changes in amplitude or total heat transport. Pfeffer *et al.* (1980) consider SV to comprise a broadly oscillatory variation of the radial energy distribution within the dominant azimuthal wavenumber component, but with relatively small variations in total energy. Buzyna *et al.* (1984) further characterize SV as a semi-periodic state which seems to form an intermediate stage towards the emergence of fully developed irregular flow or geostrophic turbulence.

Although the thermal measurements in the present study cannot distinguish variations in the radial direction, the signature at mid-radius does show a weak fluctuation in the amplitude of the dominant wavenumber and a rather stronger relative fluctuation in the amplitude of the first and higher azimuthal harmonics ($m = 6, 9$ etc.). This would seem to suggest that Pfeffer *et al.*'s (1980) characterization is somewhat incomplete. A corresponding, though weak ($\eta \sim 0.01$), fluctuation is also observed in the total heat transport (see figure 2*d*), all taking place with a period of around $20\tau_0$ (where $\tau_0 = 2\pi/\Omega$).

A particularly striking result of the present work is the suddenness at which the SV state sets in from a steady drifting wave as parameters are changed. Figure 14 shows a set of extracts from heat transport time series, $N(t)$, and their corresponding power spectra at three points closely spaced in parameter space spanning this transition. The onset of SV is immediately distinguished from the steady wave state by the relatively large-amplitude bursts of an apparently noisy periodic signal in N. This signal is, however, significantly aperiodic, as indicated by the broad spectral peaks observed around 0.12 and 0.24 rad s^{-1}. The smaller peak at $\omega = 0.05$ rad s^{-1} appears to be continuous with the oscillatory component previously associated with AV. Though apparently unrelated to the new SV frequency components, the component at 0.05 rad s^{-1} evidently grows anew in amplitude on moving into the fully developed SV regime.

As figure 14 indicates, the transition from a steady wave to SV is accomplished by increasing $\mathscr{T}$ (and/or reducing Θ) over a range of less than 0.5% (i.e. increasing Ω by 0.02 rad s^{-1}). At the intermediate value of $\mathscr{T}$, the time series exhibits transient bursts of SV separated by periods of long (though irregular) duration, during which the flow appears to resemble the steady wave regime. This observation would suggest that the bifurcation(s) leading to chaotic SV might follow a route to chaos via intermittency (of type I, e.g. Bergé *et al.* 1984). It was not possible, however, to investigate any finer structure associated with this transition (such as scaling behaviour in the degree of intermittency, e.g. Bergé *et al.* 1984), since this would require varying Ω in steps smaller than the present resolution of the experimental control system. A closer study of this transition should be an important component of future work.

5. Discussion

The present paper has shown evidence for two distinct regimes of flow in the thermally driven rotating annulus which appear to represent behaviour which is disordered in time but (at least partially) ordered in space, and which are each

obtained from regular flows via sharp transitions as external parameters are gradually varied. These properties, and quantitative estimates of apparent 'invariants' (such as attractor dimensions and Lyapunov exponents) from time-embedded phase portraits, are indicative of low-dimensional chaos, though of two quite different types which appear to arise from quite different dynamical mechanisms.

5.1. *Amplitude vacillation*

The characteristics of the periodic AV regime in the present study are broadly in agreement with previous work (e.g. Hide & Mason 1975; Pfeffer *et al.* 1980; Buzyna *et al.* 1984), although the observed transition to chaotic MAV does not appear to have been identified in earlier studies. Some evidence for MAV has appeared in some earlier work (Fowlis & Pfeffer 1969), though such modulations were attributed at the time to the disturbing effect of measurement probes. In the present cases, measurement probes do not appear to have a strong influence on the flow, and the chaotic MAV would seem to be a phenomenon intrinsic to the underlying dynamics.

Somewhat in contrast to the SV flows discussed below, the chaotic MAV flows are apparently robustly characterized by the 'invariants' (λ_1 and D_p) as low-dimensional chaos, which may arise from the nonlinear competition between two adjacent azimuthal wavenumber components influenced by secondary wave–wave interactions involving the zonal harmonic of the dominant wave (see §4.1). In particular, estimates of λ_1 from $T(t)$ time series are in reasonable agreement with those derived from $N(t)$, while estimates of D_p from $T(t)$ consistently exceed estimates from $N(t)$ by approximately 1, as expected from the absence of components due to wave drift in $N(t)$. The resulting MAV flows are evidently organized about a quasi-periodic state with three independent frequencies in $T(t)$ as a 'noisy 3-torus', and this essential structure does not appear to vary significantly within the MAV regime, even though the winding number ω_v/ω_m may vary considerably in parameter space.

The occurrence of 'noisy periodic' chaos (and of a quasi-periodic period-3 modulation 'window') is strongly reminiscent of some of the examples of 'baroclinic chaos' obtained by Hart (1985, 1986) and Ohlsen & Hart (1989*a*) in a mechanically forced two-layer system. Indeed, the superficial appearance of phase portraits from $T(t)$ and $N(t)$ in figures 5 and 6 bear a strong resemblance to some of the results of Hart (1985), with our $T(t)$ forming the counterpart to Hart's 'wave probe' data and our $N(t)$ roughly equivalent to Hart's zonal flow data, which might suggest a common mechanism for chaos in two-layer and continuously stratified flows. Upon comparison of linear return maps from the zonal flow ($N(t)$) data, however, the apparent resemblance between these two forms of noisy periodic flow is shown to be false. Hart's return maps have a roughly parabolic form with a mid-range extremum, suggestive of the logistic map, whereas our $N(t)$ return maps (figure 8*b*) show a double-valued elliptical form indicative of an underlying torus, revealing a qualitatively different mechanism for chaotic behaviour. In addition, Hart observed clear evidence for a period-doubling cascade in the transition sequence to chaos in his experiments. No evidence for period doubling was found in the present work, though it may be that the route followed here in parameter space (i.e. keeping the Grashof number constant) made such a phenomenon difficult to distinguish.

Some of the clearest examples in the experimental literature of period-doubling cascades from initially quasi-periodic flows are found in the work of Libchaber, Fauve & Laroche (1983), who detect such cascades following frequency locking of the original modes. In the present system, this would presumably require following a route in parameter space that maintained the principal ('bare') winding number

(ω_v/ω_m) constant while nonlinearity was increased. As the discussion of §4.2 indicates, this would appear to entail following a route which keeps $\Theta\mathscr{T}^{-\frac{1}{4}}$ approximately constant; a route which would require simultaneous and continuous variation of both ΔT and Ω. Such a route was beyond the scope of the present experimental control system, but should be investigated in future experimental work.

In fact, the transition to chaotic MAV in the present work would seem to have more in common with the so-called 'mode-softening' route to chaos (Langford *et al.* 1980), described for the Rayleigh–Bénard system with a magnetic field by Libchaber *et al.* (1983). In these experiments, an initially periodic state underwent a Hopf bifurcation to a quasi-periodic state with the addition of a new component at very low frequency. An increase in Rayleigh number Ra led to a steady decrease in the frequency of the new component until chaotic behaviour set in at a well-defined value of Ra. Libchaber *et al.* (1983) conjectured that this behaviour was associated with the interaction of an oscillatory mode and a stationary, symmetry-breaking instability; the very low-frequency oscillation arises from the competition between these two modes and chaos arises in association with the presence of a homoclinic orbit (e.g. Langford *et al.* 1980).

In the present case, the oscillatory mode is clearly identified with the periodic AV of $m = 3$. Symmetry breaking is found to occur at the onset of MAV in association with the occurrence of azimuthal sidebands ($m = 2$ and 4), both of which (with $m = 3$) have the same average drift frequency, and are therefore stationary with respect to a certain frame of reference. Because the transitions to chaos observed in Hart's (1985, 1986) and Ohlsen & Hart's (1989*a*) experiments were mainly from flows in which $m = 1$ or $m = 2$ were initially dominant, symmetry breaking associated with the presence of non-harmonic azimuthal sidebands did not occur (since the sidebands were also subharmonics). An important aspect of future work will be to investigate the transition to chaotic MAV more thoroughly in the thermal annulus, following different (and more highly resolved) routes in parameter space. These studies should include cases starting from a lower dominant wavenumber ($m < 3$) in order to examine the role of different kinds of azimuthal symmetry breaking in selecting the preferred route to chaos and to examine whether transition sequences more closely similar to those found by Hart (1985), e.g. involving period-doubling cascades, could occur in the present system.

5.2. *Structural vacillation*

The other type of phenomenon which may represent a form of low-dimensional chaos (SV) is quite different in form to MAV. The characteristics of the SV regime here and the transitions leading to it are broadly in agreement with previous studies (e.g. Hide & Mason 1975; Pfeffer *et al.* 1980; Buzyna *et al.* 1984), the most remarkable new results from the present work being to demonstrate the extreme sharpness of the steady wave/SV transition. The rapid onset of intermittent bursting oscillations evidently occurs within a relative range of Taylor number of $<0.5\%$, with some suggestion of a gradual increase in the frequency and duration of the intermittent bursts as Ω is increased. The resulting SV state appears to be immediately chaotic with $\lambda_1 > 0$ and $D_p \sim 3$, with no intervening quasi-periodic state. There is, however, some doubt as to whether we have been able to characterize robustly an invariant attractor dimension for the SV flows. Phase portraits within the SV regime show little structure apart from an irregular broadening of the underlying limit cycle in temperature variations associated with the drift of the dominant wave, and evidence

for some irregular cyclic behaviour in the total heat transport. Dimension estimates for T and N in this regime are not in particularly good agreement, especially at high values of Ω. It therefore remains an open question as to whether the apparent plateau in D_p for T in figure 7(*a*) is a true estimate of the appropriate attractor dimension, or represents even a lower limit.

It cannot be ruled out, for example, that the apparently chaotic behaviour observed with SV is not deterministic chaos in the accepted sense, but may represent transient quasi-chaotic behaviour, perhaps intermittently exploring a high-dimensional space at low amplitude along the lines discussed, e.g. by Tavakol & Tworkowski (1988) or Crutchfield & Kaneko (1988). The latter associate extensive transient activity with the growth of disturbances in spatially extended systems. In annulus systems such as investigated herein, SV seems often to entail the development of small-scale disturbances within the larger scale near-steady wave patterns (e.g. see HWCJS). It would be of interest to determine from more detailed measurements (and ideally, numerical simulations; see below) the extent to which such disturbances behave as independent locally evolving (as opposed to normal mode) features. It is worth remarking also that the possible importance of locally evolving disturbances (i.e. which are not normal modes) in the growth of forecast errors in atmospheric weather prediction models is becoming increasingly recognized (e.g. Farrell 1989), and may result in the intermittent transient growth of disturbances at super-exponential rates. Such behaviour renders the concept of a finite-dimensional attractor, with its spectrum of Lyapunov exponents, inadequate as a characterization of the flow.

5.3. *Chaos or 'noise amplification'?*

In both the SV and MAV transitions to chaos, a matter for some concern is the extent to which the behaviour of certain characteristics of the flows become strongly sensitive to the external parameters. In the case of SV, intermittent chaotic bursts were found to begin to occur after changing Ω by only 0.01 rad s^{-1}. For MAV, it was found in §4.2 that the modulation frequency ω_m varied approximately as $R^{-8.7}$, and that the winding number ω_v/ω_m varied roughly as $\Theta^{-8.7}\mathscr{T}^{-1.6}$.

If the observation of phenomena intrinsic to the underlying dynamics demands that external conditions be maintained constant to tolerances compatible with these sensitivities, such a requirement would place a considerable strain upon the performance of any experimental control system, especially in a rotating frame for periods extending to many hours. In particular, one might envisage the appearance of intermittent SV as due simply to slow random drifts in Ω and/or ΔT which might cause the system sporadically to cross a bifurcation point. For the MAV form of baroclinic chaos, the extreme sensitivity of winding number W to ΔT and (especially) to Ω might even suggest that the appearance of slow aperiodic behaviour was due simply to the amplification of random drifts in external parameters.

In the latter case, the clear evidence suggesting that MAV is characterizable as a form of low-dimensional chaotic behaviour, with robust λ_1 and (less certainly) D_p over a significant range of Θ and $\mathscr{T}$, would seem to indicate that the effects of random drifts (presumably implying a high intrinsic dimension) do not dominate the behaviour of the observed flow. It is important to make the cautionary remark, however, that it is difficult in principle to rule out the effects of such drifts in external parameters in determining flow behaviour from a consideration of our laboratory experiments and measurements alone. The assertion that the phenomena discussed here can be interpreted as intrinsic to the internal dynamics of the annulus would be

considerably strengthened by a demonstration that such phenomena can be successfully simulated in a numerical model, for which external parameters can be maintained constant and noise-free almost to arbitrary precision. Direct simulation of the chaotic vacillations discussed here, for example, would provide a considerable challenge to a full Navier–Stokes simulation model of annulus flows (e.g. see HWCJS), though the rewards from a successful simulation in terms of diagnostic information and subsequent dynamical insight would be very worthwhile. At a less ambitious level, the use of simpler, spectrally truncated low-order models in attempts to reproduce transition sequences and qualitatively similar forms of baroclinic chaos to our experiments could also provide valuable insight into possible mechanisms for chaotic behaviour.

5.4. *Low-order models*

The periodic vacillations and apparent transitions to low-dimensional chaotic behaviour in the present work indicate that the initial stages in the development of disordered baroclinic wave motions are a form of 'weak turbulence'. The essence of the dynamics, including typical sequences of flow transitions, should therefore be capable, at least in principle, of being captured in a 'low-order' model with a small number of degrees of freedom.

Various studies have examined the development of periodic vacillations leading to chaos in highly truncated spectral models of baroclinic waves. Pedlosky (1970, 1971) has discussed the development of a form of amplitude vacillation in a weakly nonlinear model comprising a single zonal wave mode interacting with a zonal flow with two-layer vertical discretization. This work was subsequently extended by Gibbon & McGuinness (1980) and Pedlosky & Frenzen (1980) to consider the transition to chaos, in which similarities to the well-known Lorenz equations (Lorenz 1963*a*) were found, including period-doubling cascades, a chaotic region and a sequence of period-halving bifurcations as dissipation was varied. Similar periodic amplitude vacillations were found in a continuously stratified fluid with a weakly nonlinear Eady model comprising a single zonal wavenumber mode and a baroclinic zonal flow by Drazin (1970). Transitions to chaotic behaviour in this model, also with similarities to the Lorenz set, were found by Brindley & Moroz (1980).

All these studies were limited, however, to disturbances of unrealistically small amplitude at very weak supercriticality, interacting with highly singular zonal flow states (either two-layer or continuously stratified flows with no lateral shear and zero interior gradient of potential vorticity). Furthermore, their similarity to the Lorenz set is restricted only to certain asymptotic parametric limits. In contrast, other studies have considered spectrally truncated models of baroclinic waves which are not limited to weak supercriticality, though also invoke unrealistic and singular zonal flow states. Hart (1986), for example, considered a single wave/zonal flow model with two-layer vertical structure, in which a transition to chaotic motion via a period-doubling cascade was obtained, through the chaotic attractor differed significantly from that of the Lorenz model. Weng, Barcilon & Magnan (1986) considered a nonlinear Eady model with a single zonal wavenumber component, but with up to two lateral wavenumber modes, each interacting with a baroclinic zonal flow. This model was able to capture both an AV and a form of SV (the latter entailing an exchange of energy between the radial wavenumber modes). Transitions to chaos again involved period-doubling cascades. None of these single zonal wavenumber models, however, was able to exhibit behaviour comparable with either form of chaotic motion identified here.

Boville (1982) discussed some mixed-wave aperiodic vacillations in a fully nonlinear two-layer quasi-geostrophic model with moderate spectral resolution, in which MAV were obtained with some apparent similarities to our MAV and phase-locked mixed-wave AV regimes (cf. cases i–ii). His case at $r = 0.08$, $V = 12$ m s^{-1}, for example, showed a flow dominated by $m = 3$ with an AV whose modulation index varied slowly and erratically with time, and in which the $m = 2$ sideband and $m = 1$ were also present and vacillating with the same mean frequency as $m = 3$. The phase relationships between the vacillations of $m = 1$–3 were not the same as observed in our experiments, however, and Boville's analysis did not examine the zonal phase drift of the wave components, the properties of the underlying attractor or the detailed transition sequences in sufficient detail to establish whether his model actually simulated our experiments. The apparent resemblance is, however, sufficiently close to merit further investigation.

The experimental transition to chaos via SV has not been found in any simple low-order model studied to date, and there remains a clear need for more focused modelling studies, probably using less severely truncated quasi-geostrophic models, in order to elucidate further the essential dynamics of the observed flows.

It is a pleasure to thank Professor R. Hide for his support and encouragement during this work and for many lively discussions. We are also grateful to Dr P. Hignett and W. D. N. Jackson for their contribution to the development of the apparatus, to Drs D. Broomhead and L. Smith for helpful discussions concerning the analysis of the data, and to anonymous referees for their comments in helping to improve the paper's presentation.

REFERENCES

Bergé, P., Pomeau, Y. & Vidal, C. 1984 *Order in Chaos*. Wiley.

Boville, B. A. 1982 Strongly nonlinear vacillation in baroclinic waves. *J. Atmos. Sci.* **39**, 1227–1240.

Brindley, J. & Moroz, I. M. 1980 Lorenz attractor behaviour in a continuously stratified baroclinic fluid. *Phys. Lett.* **77A**, 441–444.

Broomhead, D. & King, G. P. 1986 Extracting qualitative dynamics from experimental data. *Physica* **20D**, 217–236.

Broomhead, D., Jones, R. & King, G. P. 1987 Topological dimension and local coordinates from time series data. *J. Phys.* A: *Math. Gen.* **20**, L563–L569.

Buzyna, G., Pfeffer, R. L. & Kung, R. 1984 Transition to geostrophic turbulence in a rotating differentially heated annulus of fluid. *J. Fluid Mech.* **145**, 377–403.

Buzyna, G., Pfeffer, R. L. & Kung, R. 1989 Kinematic properties of wave amplitude vacillation in a thermally driven rotating fluid. *J. Atmos. Sci.* **46**, 2716–2729.

Cehelsky, P. & Tung, K. K. 1987 Theories of multiple equilibria and weather regimes – a critical reexamination. Part II: baroclinic two-layer models. *J. Atmos. Sci.* **44**, 3282–3303.

Crutchfield, J. P. & Kaneko, K. 1988 Are attractors relevant to turbulence? *Phys. Rev. Lett.* **60**, 2715–2718.

Curry, J. H., Herring, J. H., Loncaric, J. & Orszag, S. A. 1984 Order and disorder in two- and three-dimensional Bénard convection. *J. Fluid Mech.* **147**, 1–38.

Drazin, P. G. 1970 Nonlinear baroclinic instability of a continuous zonal flow. *Q. J. R. Met. Soc.* **96**, 667–676.

Eckmann, J.-P. & Ruelle, D. 1985 Ergodic theory of chaos and strange attractors. *Rev. Mod. Phys.* **57**, 617–656.

Farmer, J. D., Ott, E. & Yorke, J. 1983 Dimension of chaotic attractors. *Physica* **7D**, 153–180.

FARRELL, B. F. 1989 Optimal excitation of baroclinic waves. *J. Atmos. Sci.* **46**, 1193–1206.

FOWLIS, W. W. & PFEFFER, R. L. 1969 Characteristics of amplitude vacillation in a rotating, differentially-heated fluid determined by a multi-probe technique. *J. Atmos. Sci.* **26**, 100–108.

GIBBON, J. D. & MCGUINNESS, M. J. 1980 A derivation of the Lorenz equations for some unstable dispersive physical systems. *Phys. Lett.* **77A**, 295–299.

GRASSBERGER, P. & PROCACCIA, I. 1983 Characterization of strange attractors. *Phys. Rev. Lett.* **50**, 346–349.

GUCKENHEIMER, J. & BUZYNA, G. 1983 Dimension measurements for geostrophic turbulence. *Phys. Rev. Lett.* **51**, 1438–1441.

HART, J. E. 1969 Finite amplitude baroclinic instability. *Ann. Rev. Fluid Mech.* **11**, 147–172.

HART, J. E. 1985 A laboratory study of baroclinic chaos on the f-plane. *Tellus* **37A**, 286–296.

HART, J. E. 1986 A model for the transition to baroclinic chaos. *Physica* **20D**, 350–362.

HIDE, R. & MASON, P. J. 1975 Sloping convection in a rotating fluid. *Adv. Phys.* **24**, 47–100.

HIDE, R., MASON, P. J. & PLUMB, R. A. 1977 Thermal convection in a rotating fluid subject to a horizontal temperature gradient: spatial and temporal characteristics of fully-developed baroclinic waves. *J. Atmos. Sci.* **34**, 930–950.

HIGNETT, P. 1982 A note on the heat transfer by the axisymmetric thermal convection in a rotating fluid annulus. *Geophys. Astrophys. Fluid Dyn.* **19**, 293–299 (referred to as H82).

HIGNETT, P. 1985 Characteristics of amplitude vacillation in a differentially heated rotating fluid annulus. *Geophys. Astrophys. Fluid Dyn.* **31**, 247–281 (referred to as H85).

HIGNETT, P., WHITE, A. A., CARTER, R. D., JACKSON, W. D. N. & SMALL, R. M. 1985 A comparison of laboratory measurements and numerical simulations of baroclinic wave flows in a rotating cylindrical annulus. *Q. J. R. Met. Soc.* **111**, 131–154 (referred to herein as HWCJS).

JAMES, I. N., JONAS, P. R. & FARNELL, L. 1981 A combined laboratory and numerical study of fully developed steady baroclinic waves in a cylindrical annulus. *Q. J. R. Met. Soc.* **107**, 51–78.

JONAS, P. R. 1981 Some effects of boundary conditions and fluid properties on vacillation in thermally-driven rotating flow in an annulus. *Geophys. Astrophys. Fluid Dyn.* **18**, 1–23.

LANGFORD, W. F., ARNEODO, A., COULLET, P., TRESSER, C. & COSTE, J. 1980 A mechanism for a soft mode instability. *Phys. Lett.* **78A**, 11–14.

LIBCHABER, A., FAUVE, S. & LAROCHE, C. 1983 Two-parameter study of the routes to chaos. *Physica* **7D**, 73–84.

LORENZ, E. N. 1963*a* Deterministic non-periodic flow. *J. Atmos. Sci.* **20**, 130–141.

LORENZ, E. N. 1963*b* The mechanics of vacillation. *J. Atmos. Sci.* **20**, 448–464.

MAYER-KRESS, G. (Ed.) 1986 *Dimensions and Entropies in Chaotic Systems.* Springer.

NESE, J. M., DUTTON, J. A. & WELLS, R. 1987 Calculated attractor dimensions for low-order spectral models. *J. Atmos. Sci.* **44**, 1950–1972.

OHLSEN, D. R. & HART, J. E. 1989*a* The transition to baroclinic chaos on the β-plane. *J. Fluid Mech.* **203**, 23–50.

OHLSEN, D. R. & HART, J. E. 1989*b* Nonlinear interference vacillation. *Geophys. Astrophys. Fluid Dyn.* **45**, 213–235.

PEDLOSKY, J. 1970 Finite amplitude baroclinic waves. *J. Atmos. Sci.* **27**, 15–30.

PEDLOSKY, J. 1971 Finite amplitude baroclinic waves with small dissipation. *J. Atmos. Sci.* **28**, 587–597.

PEDLOSKY, J. 1987 *Geophysical Fluid Dynamics.* Springer.

PEDLOSKY, J. & FRENZEN, C. 1980 Chaotic and periodic behavior of finite-amplitude baroclinic waves. *J. Atmos. Sci.* **37**, 1177–1196.

PFEFFER, R. L., BUZYNA, G. & KUNG, R. 1980 Time-dependent modes of behavior of thermally driven rotating fluids. *J. Atmos. Sci.* **37**, 2129–2149.

RAND, D. 1982 Dynamics and symmetry: predictions for modulated waves in rotating fluids. *Arch. Rat. Mech. Anal.* **79**, 1–37.

SMITH, L. 1988 Intrinsic limits on dimension calculations. *Phys. Lett.* **133A**, 283–288.

TAKENS, F. 1980 Detecting strange attractors in turbulence. In *Dynamical Systems and Turbulence* (ed. D. Rand & L. S. Young). Lecture Notes in Mathematics, vol. 898, pp. 366–381. Springer.

TAVAKOL, R. K. & TWORKOWSKI, A. S. 1988 Fluid intermittency in low dimensional deterministic systems. *Phys. Lett.* **126**, 318–324.

WENG, H.-Y., BARCILON, A. & MAGNAN, J. F. 1986 Transitions between baroclinic flow regimes. *J. Atmos. Sci.* **43**, 1760–1777.

WHITE, H. D. & KOSCHMIEDER, E. L. 1981 Convection in a rotating, laterally heated annulus. Pattern velocities and amplitude oscillations. *Geophys. Astrophys. Fluid Dyn.* **18**, 301–320.

WOLF, A., SWIFT, J. B., SWINNEY, H. L. & VASTANO, J. A. 1985 Determining Lyapunov exponents from a time series. *Physica* **16D**, 285–317.